
Masters Theses

Student Theses and Dissertations

Fall 2016

Design methodology for behavioral surface roughness modeling and high-speed test board design

Xinyao Guo

Follow this and additional works at: https://scholarsmine.mst.edu/masters_theses



Part of the [Electrical and Computer Engineering Commons](#)

Department:

Recommended Citation

Guo, Xinyao, "Design methodology for behavioral surface roughness modeling and high-speed test board design" (2016). *Masters Theses*. 7599.

https://scholarsmine.mst.edu/masters_theses/7599

This thesis is brought to you by Scholars' Mine, a service of the Missouri S&T Library and Learning Resources. This work is protected by U. S. Copyright Law. Unauthorized use including reproduction for redistribution requires the permission of the copyright holder. For more information, please contact scholarsmine@mst.edu.

DESIGN METHODOLOGY FOR BEHAVIORAL SURFACE ROUGHNESS
MODELING AND HIGH-SPEED TEST BOARD DESIGN

by

XINYAO GUO

A THESIS

Presented to the Faculty of the Graduate School of the
MISSOURI UNIVERSITY OF SCIENCE AND TECHNOLOGY

In Partial Fulfillment of the Requirements for the Degree

MASTER of SCIENCE

in

ELECTRICAL ENGINEERING

2016

Approved by

Dr. Victor Khilkevich, Advisor

Dr. James Drewniak

Dr. Jun Fan

© 2016

XINYAO GUO

All Rights Reserved

ABSTRACT

A behavioral model is introduced, which can predict low-loss and low surface roughness transmission line time- and frequency- domain performances. High data rates push for better performance of PCB transmission lines. However, the roughness of copper foil has a considerable impact on the signal integrity performance of transmission lines at high data rates and long propagation distance. Existing models for low-loss transmission line surface roughness are inadequate. A new behavioral model to represent the surface roughness has been developed. The model is applied in the design process by adding a dispersive term to the bulk dielectric permittivity to represent the loss due to the foil surface roughness. By adding a broadband dielectric model into original transmission model, time- and frequency-domain performance improvements is achieved.

Two version of high-speed PCB test board via-transition design optimization is presented, the goal is to make the working frequency up to 50GHz and also will summarize a design flow for design a high-speed board with single and differential signal traces.

ACKNOWLEDGMENTS

I would like to express my sincere gratitude to my advisor, Prof. Victor Khilkevich, and my co-advisor, Prof. James Drewniak, for their guidance throughout my master study. Prof. James Drewniak is not only my academic mentor but also a friend. His wisdom, passion, and humor always encouraged me in study and life. Prof. Victor's profound knowledge gave me a lot of inspiration in my study.

I would like especially thank Prof. Daryl Beetner, Prof. Jun Fan and Prof. David Pommerenke for their selfless dedication and advice.

It is my honor to be part of the EMC lab. In a foreign country, EMC lab is my second home. I would like to thank my lab mates. Thank you for your help in my projects, study and life. Thank you for backing me up at a difficult time and sharing the good moments with me. The time in EMC lab will be an unforgettable and precious memory.

Finally, I would like to thank my family. Without their support, I wouldn't be able to complete my study. Especially my parents, they were always there to support me, help me and cheer up me. Meng, my husband, always trusted and loved me, taking care of me all the time.

Thank you to all the people who helped me.

TABLE OF CONTENTS

	Page
ABSTRACT.....	iii
ACKNOWLEDGMENTS	iv
LIST OF ILLUSTRATIONS.....	vi
LIST OF TABLES.....	ix
 SECTION	
1. INTRODUCTION	1
2. METHODOLOGY FOR BEHAVIORAL SURFACE ROUGHNESS MODEL	2
2.1. BACKGROUND.....	2
2.2. OBJECTIVES	13
2.3. BEHAVIORAL MODEL DESIGN APPROACHES	14
3. HIGH-SPEED TEST BOARD VIA-TRANSITION OPTIMIZATION	39
3.1. BACKGROUND.....	39
3.2. VERSION I	41
3.3. VERSION II.....	49
4. CONCLUSION.....	54
BIBLIOGRAPHY.....	56
VITA.....	59

LIST OF ILLUSTRATIONS

	Page
Figure 2.1 Causality report for S-parameter: $\epsilon' = 3.34$ and $\tan\delta = 0.003$	4
Figure 2.2 Dielectric permittivity versus frequency plot: estimated dielectric mechanisms for different region	5
Figure 2.3 Current distribution in the signal; conductor and reference planes of a stripline	6
Figure 2.4 Realistic conductor roughness exhibit the tooth structure [3]	7
Figure 2.5 Simplified hemispherical shape approximating a single surface protrusion: top and side views; current direction and applied TEM field orientations shown [3]	9
Figure 2.6 Copper foil surface SEM photograph [3]	10
Figure 2.7 Cross section of a distribution of copper spheres that create a 3D rough surface in the form of copper ‘pyramids’ on a flat conductor [3].....	11
Figure 2.8 (a) Insertion loss and phase delay per inch for a 7-inch transmission line showing errors induced by the hemispherical model [1]. (b) Measured $ S_{21} $ of a rough transmission-line compared to the linear curve	13
Figure 2.9 Extraction set test board example.....	15
Figure 2.10 STD foil 3.5mils trace width two layers dielectric model in FEMAS, thickness of effective dielectric layer is $4 \cdot h_{\text{tooth}}$	16
Figure 2.11 Border dielectric layer $\tan\delta$ and ϵ' plot	16
Figure 2.12 Dielectric parameters, first-order Debye model plot.....	17
Figure 2.13 The equivalent dielectric thickness is not an additional degree of freedom validation	18
Figure 2.14 HVLP 3.5 mil modeling results	19
Figure 2.15 Tangent loss for equivalent dielectric layer plot	20
Figure 2.16 STD 3.5 mil modeling results.....	21
Figure 2.17 STD 15mil modeling results.....	22

Figure 2.18 Meagtron 6 HVLP MB 13mil frequency domain plot	23
Figure 2.19 Example of model 3 formula loss tangent plot.....	24
Figure 2.20 Megtron 6 13mil VLP MB board modeling and measurement results	24
Figure 2.21 $\tan\delta_s$ and f_s illustration plot example	26
Figure 2.22 Old Megtron6 STD 13mil trace width board	27
Figure 2.23 (a) f_s vs trace width plot with linear fitted trend (b) $\tan\delta_s$ vs. trace width plot with linear fitted trend	29
Figure 2.24 Proposed surface roughness modeling algorithm.....	30
Figure 2.25 Stripline geometry	31
Figure 2.26 Bulk dielectric modeling example.....	32
Figure 2.27 Complete $ S_{21} $ in dB vs frequency in GHz for the entire TV set.....	33
Figure 2.28 Design curves for the surface roughness behavioral model (dispersive dielectric parameters) as a function of trace width.....	34
Figure 2.29 Available boards map--extraction and validation boards	35
Figure 2.30 Simulation results for Megtron6, HVLP foil, 7.32mil trace width	36
Figure 2.31 Simulation results for Megtron6, HVLP foil, 10.45mil trace width	36
Figure 2.32 Simulation results for Megtron7, HVLP foil, 10.45mil trace width	37
Figure 2.33 Simulation results for middle-loss material, VLP foil, 9mil trace width	37
Figure 2.34 Simulation results for high-loss material, STD foil, 9.5mil trace width	38
Figure 3.1 Example of distribution of the 15 ground via columns along the test trace	40
Figure 3.2 Achieved S-parameters and TDR	40
Figure 3.3 Allegro PCB design drawing from the last version.....	41
Figure 3.4 Desired PCB stckup design	42
Figure 3.5 Single-ended 2D cross-section analysis results.....	42
Figure 3.6 Differential 2D cross-section analysis results	43
Figure 3.7 Screen shot for via-transition key elements illustration	43

Figure 3.8 Single-ended trace CST model	45
Figure 3.9 Optimized via-transition structure insertion and return loss summary	45
Figure 3.10 Optimized via-transition structure TDR results summary.....	47
Figure 3.11 Differential trace model in CST	47
Figure 3.12 Optimized differential via-transition structure insertion and return loss summary	48
Figure 3.13 Optimized differential via-transition structure TDR results summary	48
Figure 3.14 Optimized test board layout in cadence allegro	49
Figure 3.15 Version II test board stackup.....	49
Figure 3.16 2D cross-section analysis for single-ended case	50
Figure 3.17 2D cross-section analysis for differential case	50
Figure 3.18 Single-ended CST model.....	52
Figure 3.19 Insertion and return loss for different via-transition size	53
Figure 3.20 Time-domain results for different via-transition size.....	53

LIST OF TABLES

	Page
Table 2.1 Summary of 1 st order Debye model parameters	19
Table 2.2 Summary of stage 2 formula defined parameter values for all the validation cases	22
Table 2.3 Summary of the parameters which for 12 boards modeling use idea 4	28
Table 3.1 Via-transition and coaxial port impedance list	51

1. INTRODUCTION

A behavioral model, which can predict low-loss and low surface roughness transmission line time- and frequency- domain performances are introduced in Section 1. High data rates push for better performance of PCB transmission lines. However, the roughness of copper foil has a considerable impact on the signal integrity performance of transmission lines at high data rates and long propagation distance. Existing models for low-loss transmission line surface roughness are inadequate, so a new behavioral model to represent the surface roughness was developed. The model is applied in the design process by adding a dispersive term to the bulk dielectric permittivity to represent the loss due to the foil surface roughness. By adding a broadband dielectric model into the original transmission model, time- and frequency-domain performance improvement is achieved.

In Section 2, two version of high-speed PCB test board via-transition design optimization is presented, the goal is to make the working frequency up to 50GHz and also will summarize a design flow for design a high-speed board with single and differential signal traces.

2. METHODOLOGY FOR BEHAVIORAL SURFACE ROUGHNESS MODEL

2.1. BACKGROUND

TEM transmission line is composed of any two conductors that have length, which used to transport a signal from one point to another [1]. There are different kinds of TEM transmission lines; for example, parallel-plate, parallel-rounded conductor, coaxial, microstrip, stripline and so on. This thesis will focus on symmetric stripline modeling.

For signal integrity perspective, usually, there are two criteria to evaluate the transmission line performance. First, insertion and return loss analysis in the frequency domain; second, time domain response or eye diagram analysis in the time domain. Insertion loss usually express in dB, and can be calculated from transmission coefficient, $IL = -20 \log|T|$ dB. T is the transmission coefficient; it describes the amplitude, intensity or total power of a transmitted wave V_t relative to an incident wave V_i .

$$T = \frac{V_t}{V_i} = e^{-\gamma l} \quad (1-1)$$

where l is the transmission line length and γ is the propagation constant. Propagation constant is used to describe the behavior of an electromagnetic wave along a transmission line, the general expression for complex propagation constant is:

$$\gamma = \sqrt{(r + j\omega l)(g + j\omega c)} \quad (1-2)$$

There are four parameters to describe the transmission line characteristic behavior: r (resistance per unit length in Ω/m), l (inductance per unit length in H/m), g (conductance per unit length of the dielectric medium between conducting surfaces in S/m), c (capacitance per unit length between conducting surfaces in F/m). For low-loss

case, one can assume that $R \ll \omega L$ and $G \ll \omega C$, which means R's and G's can be eliminated for γ calculation, but for the lossy case, γ need to include R's and G's.

The propagation constant gamma also can be expressed as

$$\gamma = \alpha + j\beta \quad (1-3)$$

where α is the attenuation constant (loss factor) and β is the phase constant. The loss factor can be in turn separated into conductor and dielectric loss, $\alpha = \alpha_c + \alpha_d$, depending on the parameters of corresponding materials. The specific material property causes energy loss in the dielectric named dielectric loss. The energy loss in the conductor for both signal and return path is named conductor loss.

For low-loss transmission lines alpha and beta can be expressed as [25]

$$\begin{aligned} \alpha &\approx \frac{1}{2} \left(\frac{r}{Z_0} + gZ_0 \right) \\ \beta &\approx \omega \sqrt{lc} \end{aligned} \quad (1-4)$$

with $\alpha_c = \frac{1}{2} r/Z_0$ and $\alpha_d = \frac{1}{2} gZ_0$. The dielectric dissipation factor can be rewritten as [25]

$$\alpha_d = \omega \tan \delta \quad (1-5)$$

where $\tan \delta$ is the dielectric loss tangent, it is the ratio of imaginary and real parts of the dielectric permittivity:

$$\tan \delta = -\varepsilon''/\varepsilon' \quad (1-6)$$

Therefore, in order to calculate the dissipation factor due to dielectric loss, one needs to know the permittivity of the material. There are several ways to model the dielectric permittivity, for the example frequency independent model, or measure the dielectric permittivity at several frequencies then fitted with frequencies, but all these model will cause non-causal behavior. Figure 2.1 shows an in-house tool check S-

parameter causality results, the S-parameter also calculated use in-house tool, the parameter values used for S-parameter calculation are $\epsilon' = 3.34$ and $\tan\delta = 0.003$.

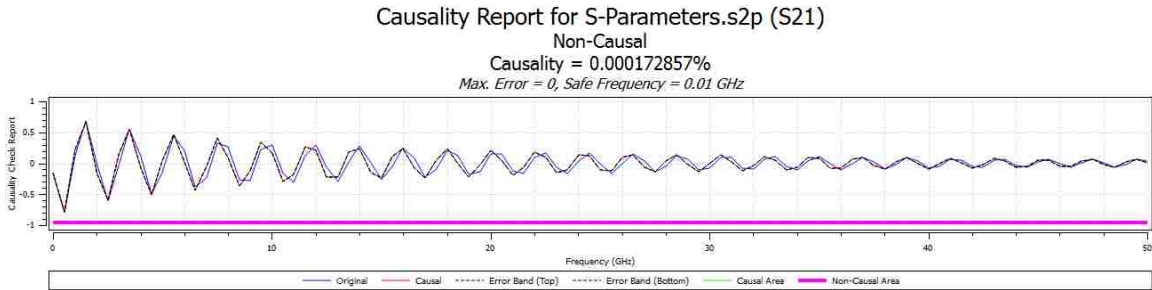


Figure 2.1 Causality report for S-parameter: $\epsilon' = 3.34$ and $\tan\delta = 0.003$

Dielectric permittivity can be modeled accurately in different interest frequency range by using different approaches. Figure 2.2 shows estimated dielectric mechanisms at different frequency range. From the plot observation, the low-frequency dielectric behavior can be modeled by first-order Debye mode and the high-frequency dielectric behavior can be modeled by Lorentz model, Equation 1-8. In the intermediate region, neither two of the previous model is accurate. In this article, the interesting frequency is the intermediate region, from MHz to tens of GHz. Wide-band Debye model has been chosen to imitate this region. It is a casual model and can provide sufficient accuracy for transmission line modeling up to 40GHz [19]. Equation 1-9 is wide-band Debye model expression

$$\epsilon_{Debye} = \epsilon_{\infty} + \frac{\epsilon_{DC} - \epsilon_{\infty}}{1 + j\omega\tau_{Debye}} \quad (1-7)$$

$$\epsilon_{Lorentz} = \epsilon_{\infty} + \frac{(\epsilon_{DC} + \epsilon_{\infty})\omega_0^2}{\omega_0^2 + j\omega\tau_{Lorentz} - \omega^2} \quad (1-8)$$

$$\epsilon(f) = \epsilon(\infty) + \frac{\epsilon_d}{(m_1 - m_2) \cdot \ln(10)} \left[\frac{10^{m_2 + if}}{10^{m_1 + if}} \right] \quad (1-9)$$

where $\omega_1 = 2\pi 10^{m1}$ and $\omega_2 = 2\pi 10^{m2}$ are the lower and upper frequency limit. ϵ_d and $\epsilon(\infty)$ can be obtained by one measurement of dielectric constant at measured frequency.

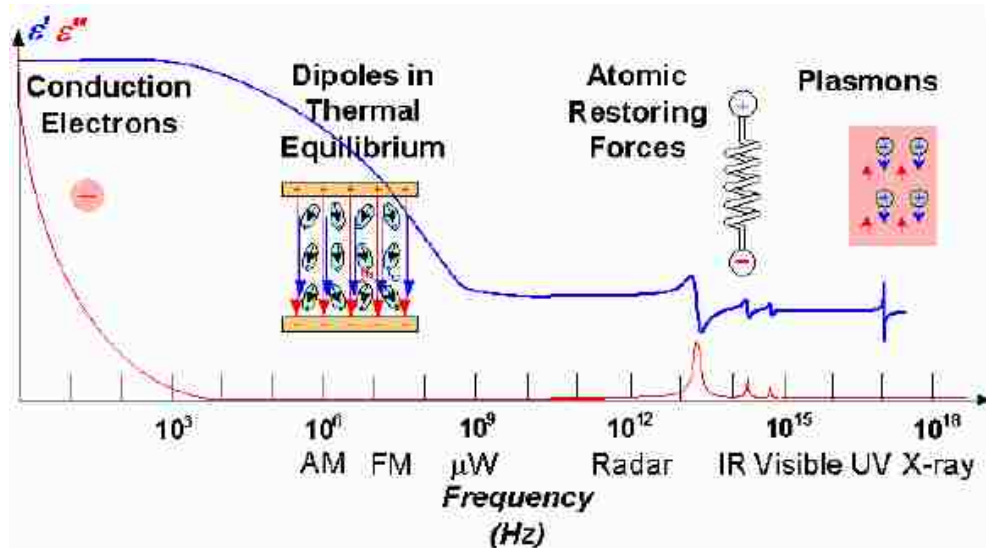


Figure 2.2 Dielectric permittivity versus frequency plot: estimated dielectric mechanisms for different region

The conductor loss is usually modeled as follows. At low frequencies, in stripline transmission lines, the current will flow through the entire cross-section of the conductors. At high frequencies, for stripline, the current are concentrated in the upper and lower edges of the conductor, as shown in Figure 2.3. The electric current flows mainly at the “skin” of the conductor, between the outer surface and a skin depth δ [2]. The skin depth formula is

$$\delta = \sqrt{\frac{2}{\omega\mu\sigma}} \quad (1-10)$$

where ω is the angular frequency, $\mu = \mu_r\mu_0$ is the permeability of the conductor, (μ_r is the relative permeability of the conductor and μ_0 is the permeability of free space), σ is metal conductivity.

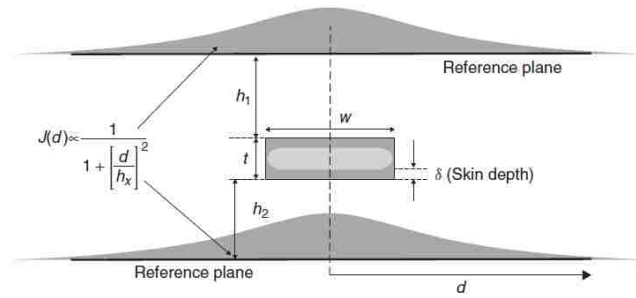


Figure 2.3 Current distribution in the signal; conductor and reference planes of a stripline

Frequency dependent total resistance for stripline include skin effect obtained by the two resistance values, resistances calculated from top and bottom reference planes, put in parallel. The resistance from top and bottom reference planes can be calculated as [3]

$$R = \sqrt{\frac{\pi \mu f}{\sigma}} \left(\frac{1}{w} + \frac{1}{6h} \right) \quad (1-11)$$

from equation (1-11) could derive stripline resistance show in below

$$R_{ac,strip} = \frac{(R_{(h1)})(R_{(h2)})}{R_{(h1)} + R_{(h2)}} \quad (1-12)$$

The realistic conductor rough surface reminds a “tooth structure”, show in Figure 2.4. When the tooth height is comparable to the skin depth, the conductor foil should be treated as the rough case [3]. There are three very common conductor surface roughness models: Hammerstad model, Hemispherical model, and Huray model.

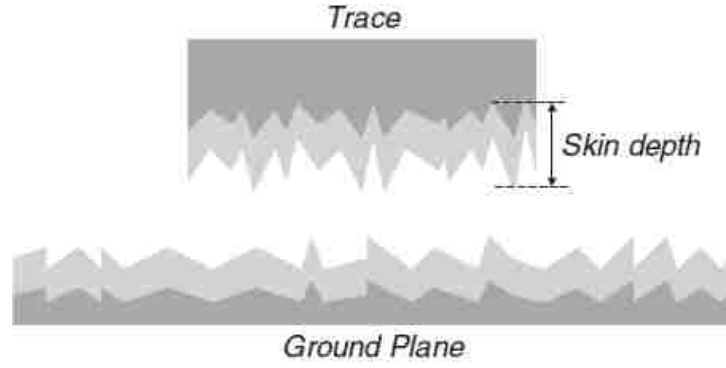


Figure 2.4 Realistic conductor roughness exhibit the tooth structure [3]

Hammerstad model is a traditional way to model conductor foil surface roughness. Hammerstad equation to model transmission line gives the following expression for PUL R due to the surface roughness losses:

$$R_{ac} = K_H R_s \sqrt{f} \quad (1-13)$$

where K_H is the Hammerstad coefficient and $R_s \sqrt{f}$ is the classic skin resistance for smooth conductor. The correction coefficient is given as follows:

$$K_H = 1 + \frac{2}{\pi} \arctan\left[1.4 \left(\frac{h_{rms}}{\delta}\right)^2\right] \quad (1-14)$$

where δ is the skin depth. Hammerstad coefficient used to represent the extra loss caused by the conductor surface roughness. Frequency dependent skin effect resistance and total inductance using the Hammerstad correction for surface roughness are presented below

$$R_H(f) = \begin{cases} K_H R_s \sqrt{f} & \text{where } \delta < t \\ R_{dc} & \text{where } \delta \geq t \end{cases} \quad (1-15a)$$

$$L_H(f) = \begin{cases} L_{external} + \frac{R_H(f)}{2\pi f} & \text{where } \delta < t \\ L_{external} + \frac{R_H(f_{\delta=t})}{2\pi f_{\delta=t}} & \text{where } \delta \geq t \end{cases} \quad (1-15b)$$

To be more accurate to model the roughness profile large than 2um, the roughness profile could be approximated as random protrusion sitting on the flat plane. Hemispherical model [3] models the complete copper surface as N separated individual protrusions randomly distributed on a flat plane, as shown in Figure 2.5. The effect of protrusions is modeled by calculating the effective cross-section area of the hemispherical protrusions:

$$\sigma_{tot} = -\frac{\pi}{k^2} \sum_m (2m+1) \text{Re}[\alpha(m) + \beta(m)] \quad (1-16)$$

where $k = 2\pi/\lambda$, and α and β are scattering coefficients. Since the protrusions are electrically small, only the first order coefficients are taken into account:

$$\alpha(1) = -\frac{2j}{3} (kr)^3 \frac{1-(\delta/r)(1+j)}{1+(\delta/2r)(1+j)} \quad (1-17a)$$

$$\beta(1) = -\frac{2j}{3} (kr)^3 \frac{1-(4j/k^2 r \delta)[1/(1-j)]}{1+(\frac{2j}{k^2 r \delta})[1/(1-j)]} \quad (1-17b)$$

where r is the sphere radius. The total absorbed or scattered power is given by:

$$P_{hemisphere} = \frac{1}{2} \left(\frac{1}{2} \eta |H_0|^2 \sigma_{tot} \right) = -\text{Re} \left[\frac{1}{4} \eta |H_0|^2 \frac{3\pi}{k^2} (\alpha(1) + \beta(1)) \right] \quad (1-18)$$

where $\eta = \sqrt{\mu_0/\varepsilon_0 \varepsilon'}$ is the impedance of the transmission line medium, and H_0 is the magnitude of applied magnetic field. The power dissipated in the flat regions surrounding the hemispheres is given by:

$$\frac{dP_{plane}}{da} = \frac{\mu_0 \omega \delta}{4} |H_0|^2 \quad (1-19)$$

The dissipated power of the protrusion on the flat plane is calculated by adding half of hemisphere dissipated power and the power absorbed by the flat plane of that hemisphere base area:

$$P_{tot} = \left| -\text{Re} \left[\frac{1}{4} \eta |H_0|^2 \frac{3\pi}{k^2} (\alpha(1) + \beta(1)) \right] \right| + \frac{\mu_0 \omega \delta}{4} |H_0|^2 (A_{tile} - A_{base}) \quad (1-20)$$

where A_{tile} is the tile area of the flat plane surrounding the protrusion, and A_{base} is the base area of the hemisphere. A_{base} and A_{tile} are illustrate in the Figure 2.3.

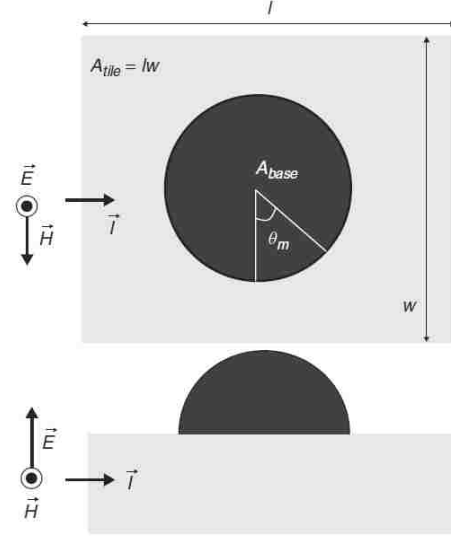


Figure 2.5 Simplified hemispherical shape approximating a single surface protrusion: top and side views; current direction and applied TEM field orientations shown [3]

To calculate the new coefficient shows in Equation (1-13), the ratio of the power absorbed with and without protrusion need to be derived. This can be obtained by dividing (1-18) and (1-20), the equation could be simplified:

$$K_s = \frac{|Re[\eta(3\pi/4k^2)(\alpha(1)+\beta(1))]| + (\mu_0\omega\delta/4)(A_{tile}-A_{base})}{\frac{\mu_0\omega\delta}{4}A_{tile}} \quad (1-21)$$

The limitation of Equation (1-21) is when the skin depth is greater than the protrusion height. Therefore, there is a knee frequency defined when $K_s = 1$. It means when the roughness begin to affect the loss significantly.

$$K_{hemi} = \begin{cases} 1 & \text{when } K_s \leq 1 \\ K_s & \text{when } K_s > 1 \end{cases} \quad (1-22)$$

The frequency dependent skin depth resistance and total inductance using in the Hemispherical model to represent the extra losses caused by surface roughness:

$$R_H(f) = \begin{cases} K_H R_s \sqrt{f} & \text{where } \delta < t \\ R_{dc} & \text{where } \delta \geq t \end{cases} \quad (1-23a)$$

$$L_H(f) = \begin{cases} L_{external} + \frac{R_{hemi}(f)}{2\pi f} & \text{where } \delta < t \\ L_{external} + \frac{R_{hemi}(f_{\delta=t})}{2\pi f_{\delta=t}} & \text{where } \delta \geq t \end{cases} \quad (1-23b)$$

Huray model was invented by Paul G. Huray in 2006 at the University of South Carolina [3]. It is a new wideband model for surface roughness, which is adequate than Hammerstad and hemisphere model, it also named ‘snowball’ model. Figure 2.6 shows the scanning electron microscope (SEM) of surface roughness sample on the printed circuit board (PCB). Figure 2.7 shows the 3D model, which was built to represent the ‘snowball’ surface.



Figure 2.6 Copper foil surface SEM photograph [3]

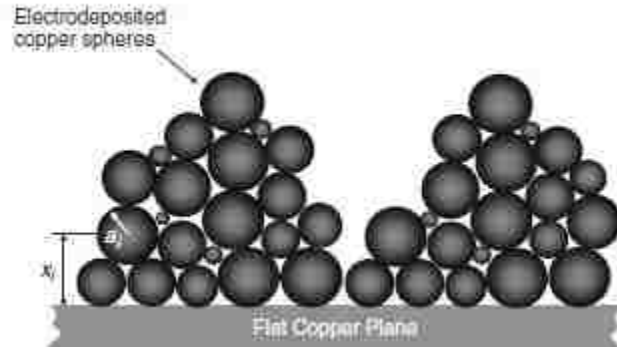


Figure 2.7 Cross section of a distribution of copper spheres that create a 3D rough surface in the form of copper 'pyramids' on a flat conductor [3]

The power dissipated on the protrusion is calculated similarly to the hemispherical model (1-18) but with twice the magnitude:

$$P_{sphere} = \left(\frac{1}{2}\eta|H_0|^2\sigma_{tot}\right) = -Re\left[\frac{1}{2}\eta|H_0|^2\frac{3\pi}{k^2}(\alpha(1) + \beta(1))\right] \quad (1-24)$$

The new correction coefficient is shown below:

$$K_{Huray} = \frac{P_{flat} + P_{N,spheres}}{P_{flat}} = \frac{|Re[\eta(3\pi/4k^2)(\alpha(1)+\beta(1))]| + (\mu_0\omega\delta/4)(A_{tile}-A_{base})}{\frac{\mu_0\omega\delta}{4}A_{tile}} \quad (1-25)$$

Huray model represents the extra loss caused by surface roughness shown below:

$$R_{Huray}(f) = \begin{cases} K_{Huray}R_s\sqrt{f} & \text{when } \delta < t \\ R_{dc} & \text{when } \delta \geq t \end{cases} \quad (1-26a)$$

$$L_{Huray}(f) = \begin{cases} L_{extrernal} + \frac{R_{Huray}(f)}{2\pi f} & \text{when } \delta < t \\ L_{extrernal} + \frac{R_{Huray}(f_{\delta=t})}{2\pi f_{\delta=t}} & \text{when } \delta \geq t \end{cases} \quad (1-26b)$$

Hammerstad model could only model the copper roughness RMS value less than about 2 μm . Hemisphere model improved the modeling results base on Hammerstad model, but still underestimated the loss at high frequencies. It can give accurate results only when to know the protrusion geometry parameter accurately, therefore not effective

for a smooth surface. Huray model can model any type of surface roughness, even the sphere size is less than 1 μm , but need to have detailed surface profile or scanning electron microscope figure.

In [16], it presents a different way to model PCB conductor surface roughness model. Instead of imitating the roughness profile, it uses an additional layer with effective material parameters to present surface roughness. This method is based on the effective medium theory. The effective medium theory describes a medium (composite material) based on the properties and the relative fraction of its components [17-18]. Conductor roughness in the proposed approach is substituted with a “roughness composite dielectric” layer. In this article, it evaluated three groups of test vehicles; in each group has nine boards. Three groups only differed in foil types (STD-standard, VLP-very-low-profile, and HVLP-hyper-very-low-profile foils). The “roughness dielectric” is modeled as a lossy non-dispersive material, the three types of foil “roughness dielectric” parameters are shown in below:

$$\begin{aligned} STD: \quad \epsilon_{STD} &= 48.5 - j18.4 \quad (\tan \delta_{STD} = 0.38); \\ VLP: \quad \epsilon_{VLP} &= 33.1 - j4.97 \quad (\tan \delta_{VLP} = 0.15); \\ HVLP: \quad \epsilon_{HVLP} &= 28.9 - j1.73 \quad (\tan \delta_{HVLP} = 0.06) \end{aligned}$$

The “roughness dielectric” in each case of a foil type has its own effective dielectric properties and thickness, depending on the roughness amplitude. This method requires using 2D cross-section analysis. The article shows that this model works up to 20GHz, the modeling results have very good correlations with measurement results, the differences are within 1dB.

2.2. OBJECTIVES

The objective of this research is to develop an accurate low-loss transmission line model, which can be used to precisely predict the actual case. Most of the existing transmission line models can model the high-loss and middle-loss transmission lines (with the dielectric loss tangent $\tan\delta$ larger than 0.01) in frequency- and time-domain adequately [5,8]. However, for low-loss material with $\tan\delta$ less than 0.01, the existing transmission line models demonstrate lack of accuracy (Figure 2.8a). Surface roughness effect is often modeled as scattering of the electromagnetic wave on protrusions of the conductor (hemispherical model [5] and snowball model [14] implemented in ADS). This approach, however, cannot model increase of the slope of transmission coefficient curve with frequency, which can be clearly observed for low-loss transmission lines [15, 19] with a typical example shown in Figure 2.8b.

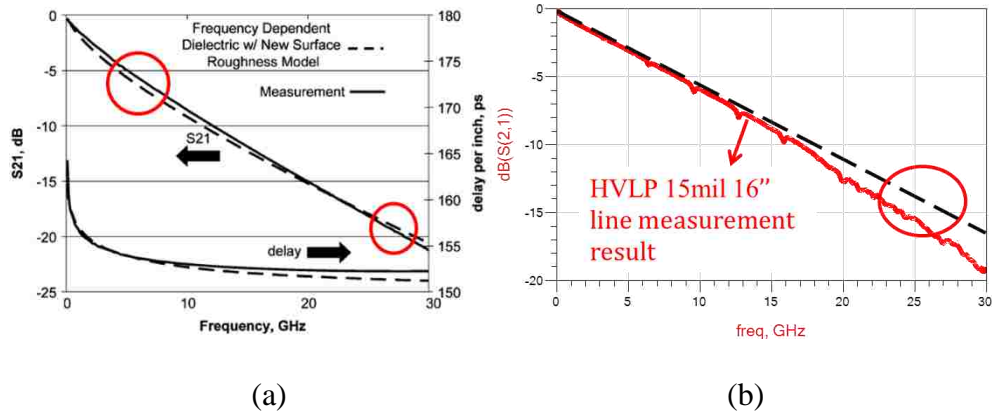


Figure 2.8 (a) Insertion loss and phase delay per inch for a 7-inch transmission line showing errors induced by the hemispherical model [1]. (b) Measured $|S_{21}|$ of a rough transmission-line compared to the linear curve

This work will present a new way to model the conductor surface roughness effect with effective dielectric. To achieve the goal two variants of the model were tested. In the first one, we used the method from [16] with the dispersive dielectric in the effective layer. In the second one instead of using effective dielectric layer, an additional term adding to the bulk dielectric, which simplifies the simulation, is eliminating the need of 2D cross-sectional analysis. In this variant of the model, the per-unit-length (PUL) parameters of transmission-line are calculated analytically to obtain the transmission coefficient of the line.

2.3. BEHAVIORAL MODEL DESIGN APPROACHES

As stated before, the existing surface roughness models are adequate to capture the high-loss and mid-loss material, which dissipation factor, $DF=\tan\delta$, is larger than 0.1. For low-loss material and low-loss surface roughness, existing model's accuracy is not enough. In [10], it mentioned that the accuracy of transmission line models usually depends on broadband dielectric and conductor roughness models. The following section will introduce two methods to model low-loss and low surface roughness transmission line. The first model using an additional dispersive layer to represent surface roughness effect and the second model is added a dispersive dielectric term, use wide-band Debye dielectric model, to represent surface roughness.

Method I – Add Additional Dispersive Dielectric Layer. This part will introduce the implemented procedures of add additional dispersive layer method, and show the model results.

For this study, a set of test vehicles (TV) was created. The set consisted of twelve boards, each having 50 ohms single-ended 16-inch striplines of three different roughness grades (STD, RTF/VLP, and HVLP) and four different widths (3.5, 9.5, 13 and 15 mils). All the boards contained a TRL pattern for de-embedding purposes and were manufactured using the same dielectric material (Megtron 6). An example of the test vehicle is demonstrated in Figure 2.9.

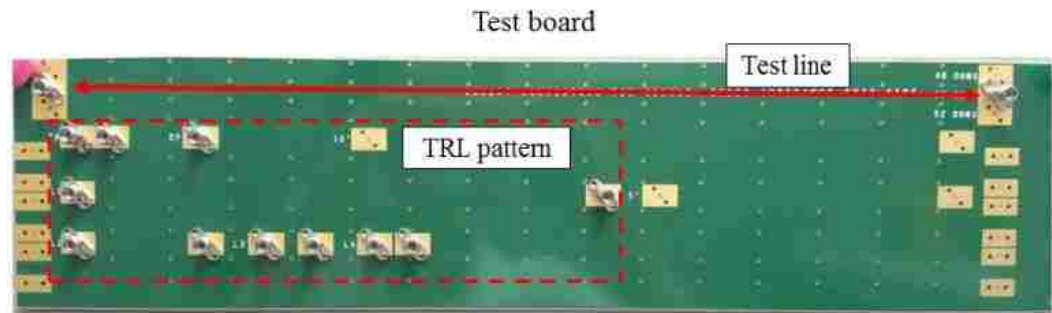


Figure 2.9 Extraction set test board example

Two layers dielectric model plot is shown in Figure 2.10. The yellow part is copper, it represents the stripline reference grounds and conductor; the blue part is the border dielectric, it represents the actual stripline dielectric; the green part is an additional dispersive dielectric layer, also named equivalent dielectric layer, it represents the surface roughness. This equivalent dielectric layer should be dispersive, frequency dependent, so it can model extra slope performance at high frequencies [10]. There are four numerical models used to model the equivalent layer dielectric parameters. Idea 1, 1st order Debye model, idea 2 is $\tan\delta = A(1 - e^{-\alpha\omega})$ and the idea 3 is $\tan\delta = A_1(1 - e^{-\alpha_1\omega}) + \frac{A_2}{1 + e^{-\alpha_2(\omega - \omega_1)}}$ and idea 4 is the combination of Debye term and Lorentz term to define dielectric permittivity.

Due to the extraction set has the same dielectric, for simplicity, in this idea assume the border dielectric is same for all extraction cases and is calculated according to the Djorivic Model [5]. Figure 2.11 shows the border dielectric layer tangent loss and real part of dielectric permittivity plot.

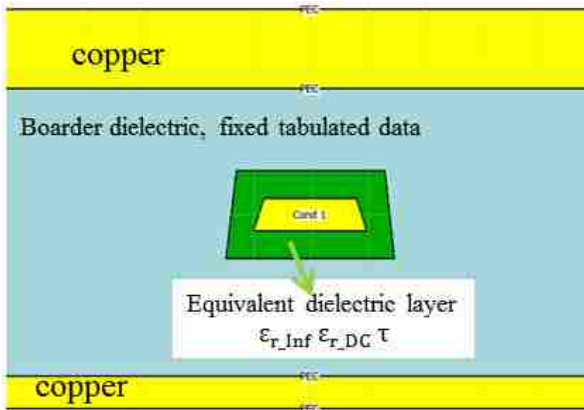


Figure 2.10 STD foil 3.5mils trace width two layers dielectric model in FEMAS, thickness of effective dielectric layer is $4 \cdot h_{tooth}$

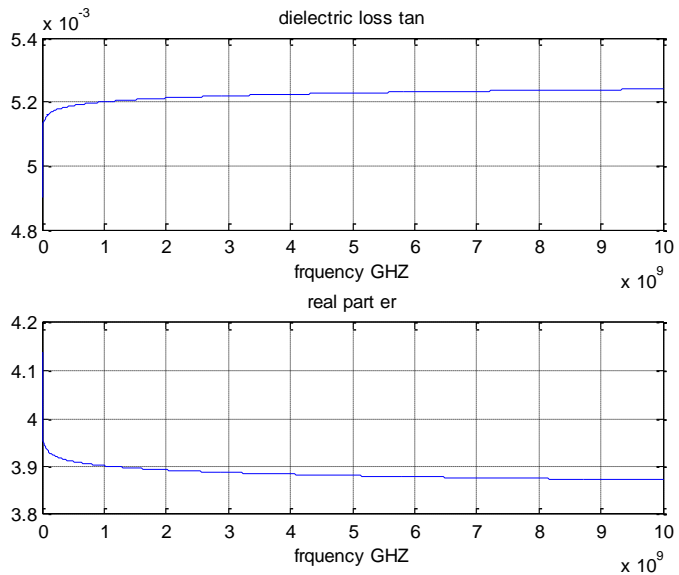


Figure 2.11 Border dielectric layer $\tan\delta$ and ϵ' plot

The border dielectric calculated in Equation (1-27). This model works in the range of $[\omega_1, \omega_2]$.

$$\text{Re}\{\varepsilon_r(\omega)\} \approx \varepsilon'_\infty + \frac{\Delta\varepsilon'}{m_1 - m_2} \frac{\ln(\frac{\omega_2}{\omega})}{\ln(10)} \quad (1-27a)$$

$$\text{Im}\{\varepsilon_r(\omega)\} \approx \frac{\Delta\varepsilon'}{m_2 - m_1} \frac{-\frac{\pi}{2}}{\ln(10)} \quad (1-27b)$$

where ε'_∞ is the real part of relative permittivity at high frequencies. $\Delta\varepsilon'$ is the variation of the real part of relative permittivity. $\omega_1 = 10^{m_1}$ and $\omega_2 = 10^{m_2}$ are the frequency lower and upper bonds.

Idea 1 first order Debye model. The expression of the equivalent dielectric layer is shown in Equation 1-28 and an example plot is shown in Figure 2.12, the equivalent dielectric parameters are $\varepsilon_{DC}=48.5$, $\varepsilon_\infty=44.71$, and $\tau=0.8e11$

$$\varepsilon = \varepsilon_\infty + \frac{\varepsilon_{DC} - \varepsilon_\infty}{1 + j\omega\tau} \quad (1-28)$$

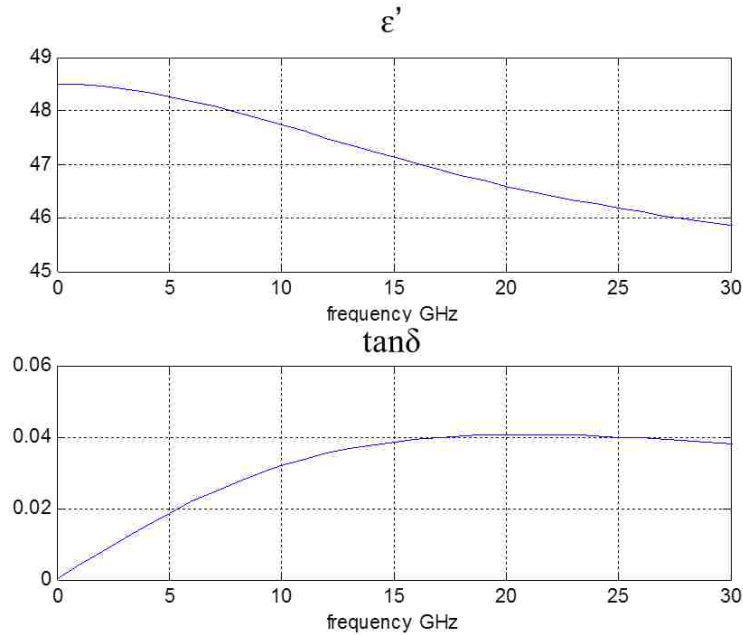


Figure 2.12 Dielectric parameters, first-order Debye model plot

Before starting to model the entire extraction set, one need to understand whether the thickness of the equivalent dielectric layer is an additional degree of freedom or not. Figure 2.13 shows that for different equivalent dielectric layer thicknesses, by tuning the Debye model parameter can have a very similar result, which means that the equivalent dielectric layer thickness is not a degree of freedom. Since this equivalent dielectric layer represents surface roughness, its thickness should be the same magnitude, in this case, the model uses four times the roughness mean square root of tooth peak ($4 \cdot h_{tooth}$) for all other cases.

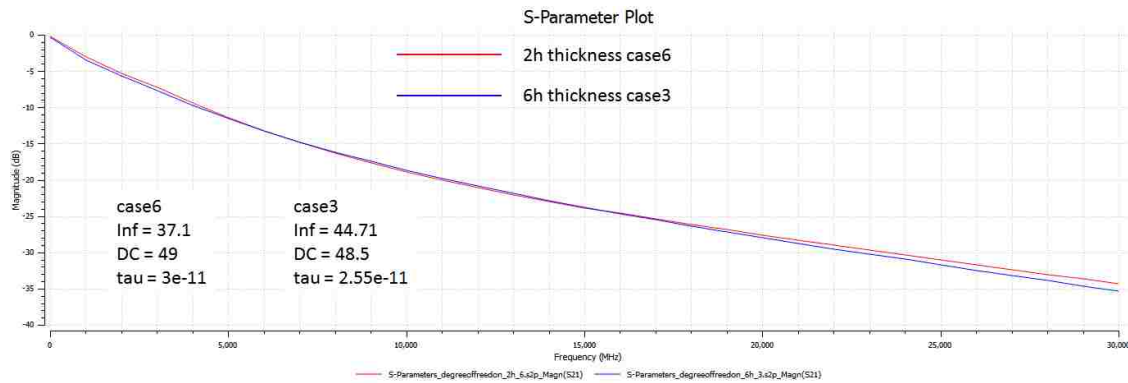


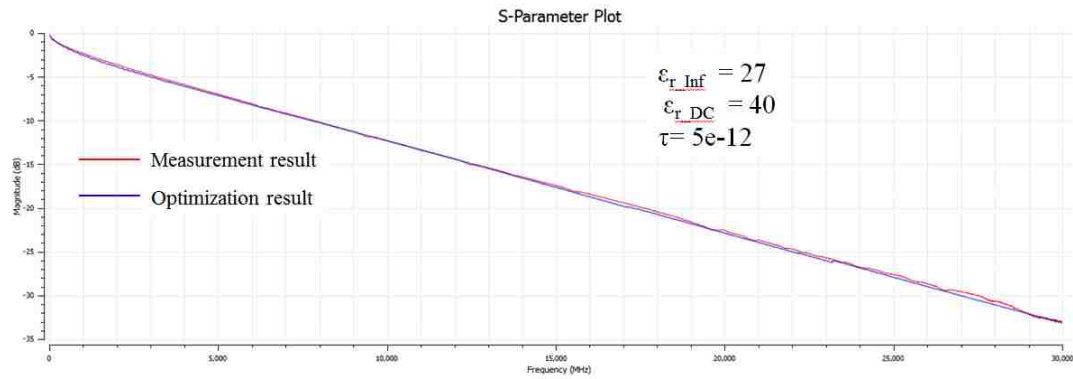
Figure 2.13 The equivalent dielectric thickness is not an additional degree of freedom validation

Eight boards were used to extract the parameters for the additional layer. Figure 2.14 shows an example of idea 1 modeling results. The modeling result has good correlation with the measurement result.

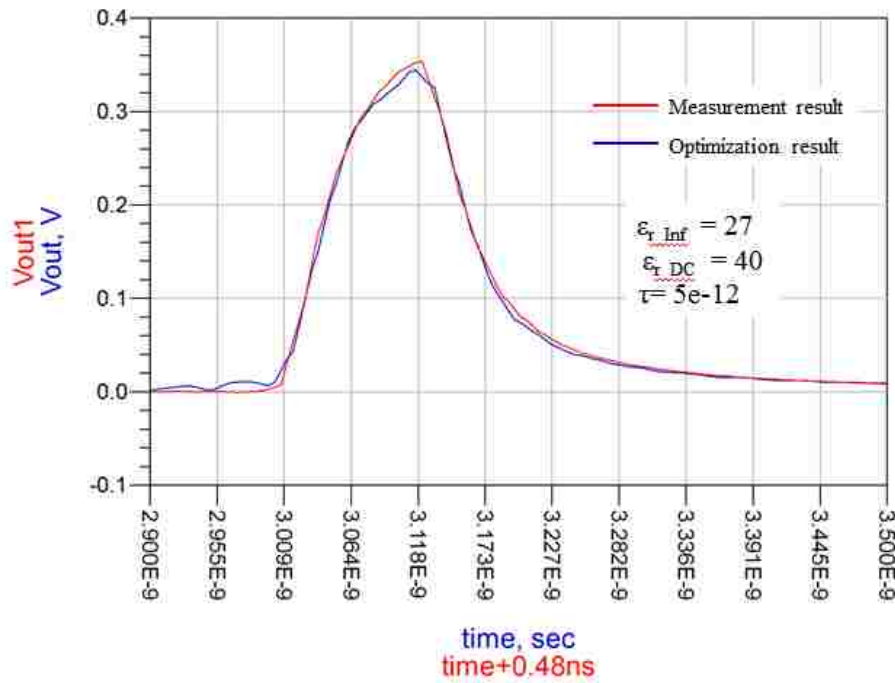
Table 2.1 shows the summary of 1st order Debye model parameters. This method only fitted for eight cases, 9.5mil standard foil did not include. The parameters as shown in this table, there are no clear clue that can be used for the future.

Table 2.1 Summary of 1st order Debye model parameters

	STD	RTF	HVLP	
3.5mil	$\epsilon_{r_Inf} = 44.71$ $\epsilon_{r_DC} = 48.5$ $\tau = 8e-12$	$\epsilon_{r_Inf} = 27.2$ $\epsilon_{r_DC} = 34$ $\tau = 7.7e-12$	$\epsilon_{r_Inf} = 23.5$ $\epsilon_{r_DC} = 34$ $\tau = 5e-12$	$\epsilon_{r_Inf} = 27$ $\epsilon_{r_DC} = 40$ $\tau = 5e-12$
9.5mil	none	$\epsilon_{r_Inf} = 28.5$ $\epsilon_{r_DC} = 33.1$ $\tau = 5e-12$	$\epsilon_{r_Inf} = 18.5$ $\epsilon_{r_DC} = 40$ $\tau = 4.8e-12$	
15mil	$\epsilon_{r_Inf} = 48.5$ $\epsilon_{r_DC} = 65.5$ $\tau = 4.8e-13$	$\epsilon_{r_Inf} = 22$ $\epsilon_{r_DC} = 36$ $\tau = 6.7e-12$	$\epsilon_{r_Inf} = 12.5$ $\epsilon_{r_DC} = 40$ $\tau = 4.6e-12$	



(a)



(b)

Figure 2.14 HVLP 3.5 mil modeling results (a) frequency domain (b) time domain

This is the first model that been used for the equivalent dielectric layer, and the modeling results are not as good as expected, the other dielectric model options should be tried first. The parameters of this model do not indicate a clear trend that can be used in the future.

Idea 2 $\tan\delta = A(1 - e^{-\alpha\omega})$. The modeling procedure is the same as in idea 1. The equivalent dielectric layer permittivity calculation replaced by $\tan\delta = A(1 - e^{-\alpha\omega})$. Unlike idea 1, this formula is only decided by two parameters, A and α . A will be the magnitude of loss tangent at high frequencies and α will decide the frequency start to become stable. Figure 2.15 shows the tangent loss behavior of idea 1 (green curve) and 2 (blue curve). First order Debye model tangent loss will drop at high frequencies which is not desired. Tangent loss should increase a little as frequency increases, which can create extra loss at high frequencies.

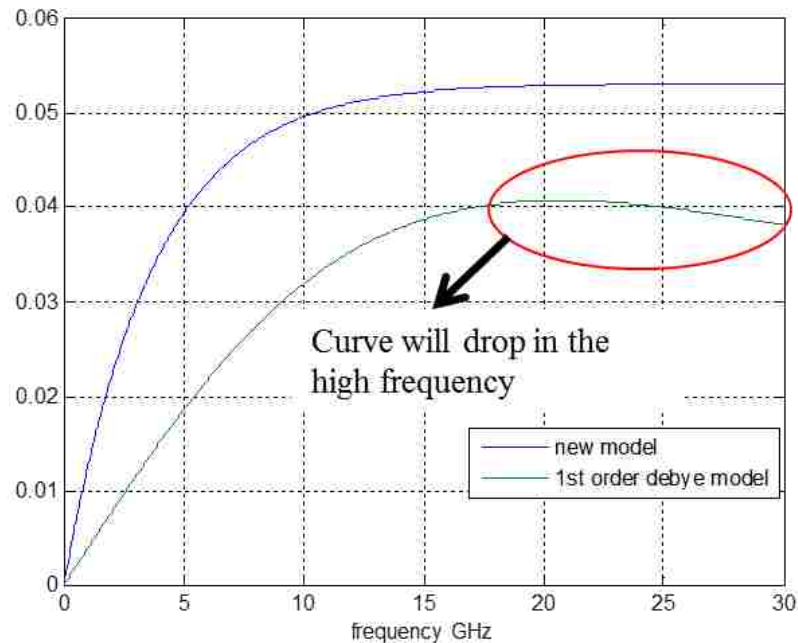
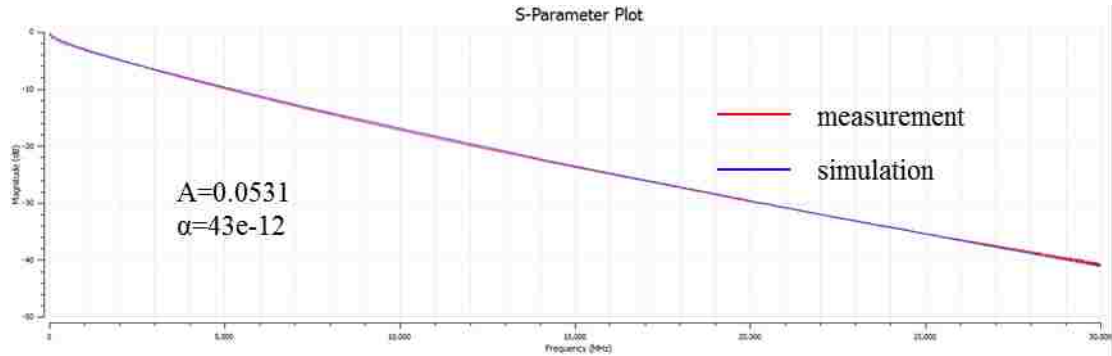
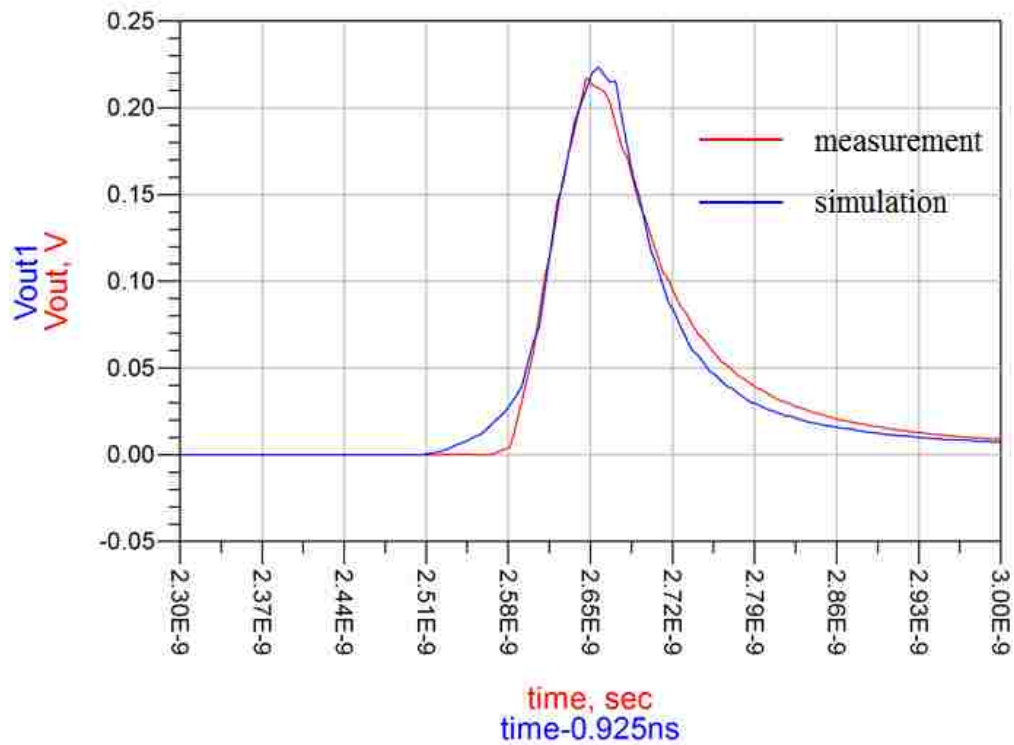


Figure 2.15 Tangent loss for equivalent dielectric layer plot

Similar to idea 1, this model also fit for all the extraction cases. The results are showing in the Table 2.2. To show how this formula improves the S-parameter correlation at high frequencies, two STD foil cases are shown. Figure 2.16 and 2.17 show the frequency-domain and time-domain modeling results for STD foil 3.5mil and 15mil.

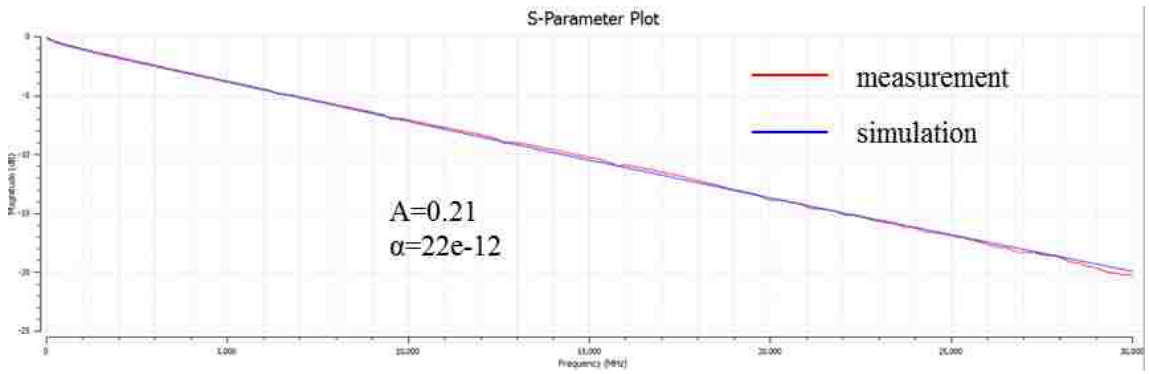


(a)

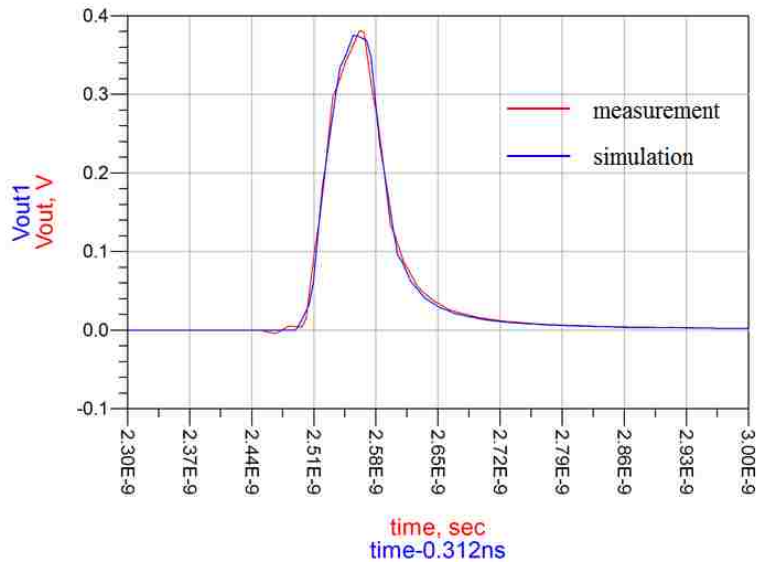


(b)

Figure 2.16 STD 3.5 mil modeling results (a)frequency domain (b) time domain



(a)



(b)

Figure 2.17 STD 15mil modeling results (a) frequency domain (b) time domain

Table 2.2 Summary of stage 2 formula defined parameter values for all the validation cases

	STD	RTF	HVLP
3.5mil	$A=0.0531$ $\alpha=43$	$A=0.125$ $\alpha=23$	$A=0.213$ $\alpha=11$
9.5mil	None	$A=0.135$ $\alpha=5.6$	$A=0.545$ $\alpha=7.9$
15mil	$A=0.21$ $\alpha=22$	$A=0.5$ $\alpha=5.2$	$A=1.5$ $\alpha=3.3$

This table shows that the idea 2 formula parameters can have a monotonic trend, but for one case, probably will have one or more A and α combinations. However, when implement idea 2 to 13mil trace width boards, it could not model very well at low frequencies and causes extra loss. Figure 2.19 shows Megtron 6 HVLP MB 13mil modeling results.

In the Figure 2.18, this model shows that it overestimates the low-frequency loss and underestimates the high-frequency loss. So one consider trying other options to see whether can achieve results that are more accurate or not by separating model the low- and high- frequency loss. In addition, this model is a non-causal model, it is not desired for later time domain analysis.

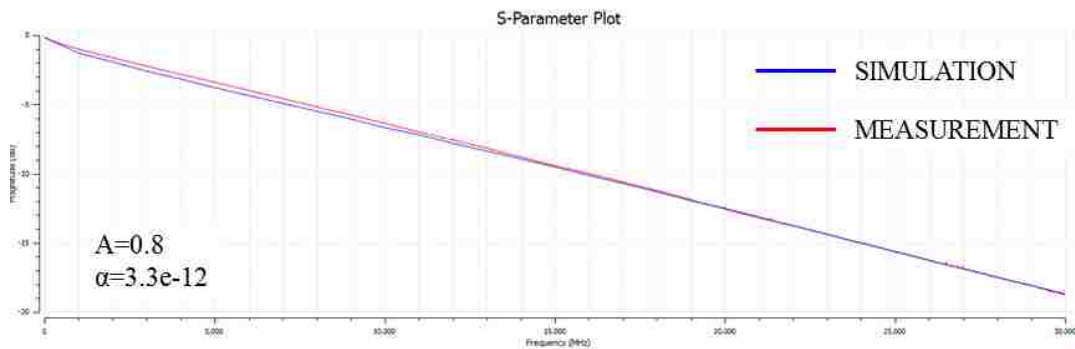


Figure 2.18 Meagtron 6 HVLP MB 13mil frequency domain plot

Idea 3 $\tan\delta = A_1(1 - e^{-\alpha_1\omega}) + A_2/(1 + e^{-\alpha_2(\omega-\omega_1)})$. In order to better model the low-loss transmission line frequency-domain behavior, the low-frequency loss and high-frequency loss modeled separately. Figure 2.19 shows an example plot for tangent loss which has two levels for low and high frequencies. A_1 is the level value for low frequencies and A_2 is the level value for high frequencies. α_1 is where the low frequencies

start to become stable and α_2 is where the high frequencies start to become stable and ω_1 is where the frequencies start the second level.

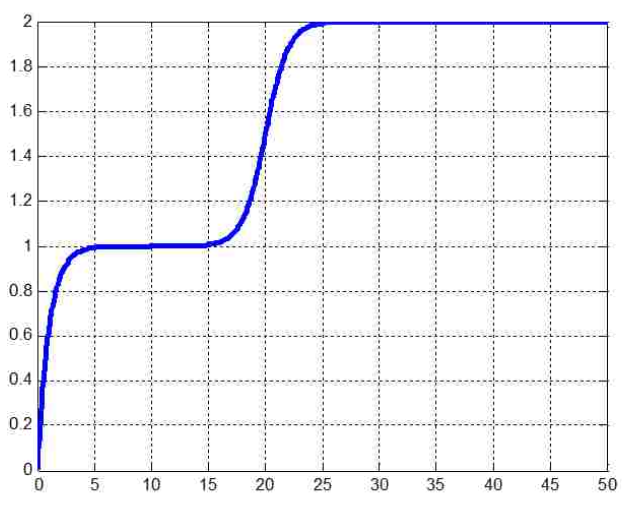


Figure 2.19 Example of model 3 formula loss tangent plot

The reason to develop this idea is to model the 13mil trace width boards well. However, after adding another degree of freedom in the formula, the modeling results do not improve as expected. Figure 2.20 shows the modeling results for Megtron 6 VLP 13mil MB board.

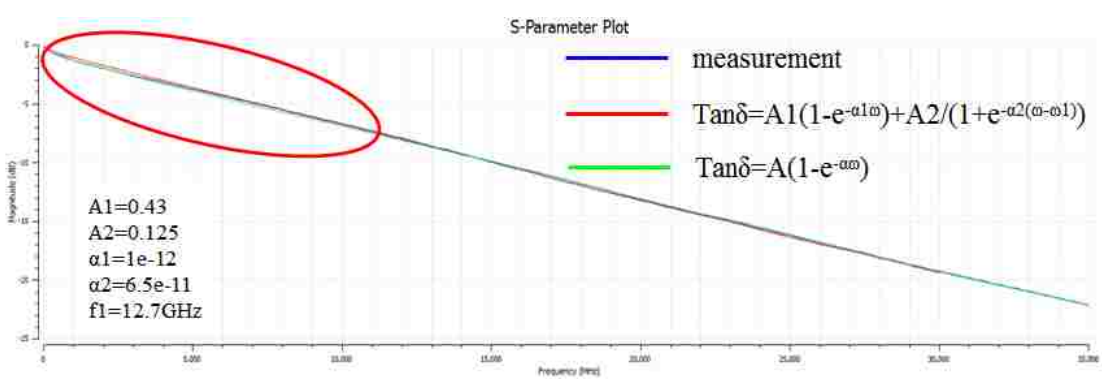


Figure 2.20 Megtron 6 13mil VLP MB board modeling and measurement results

Even though increased the model parameters, the accuracy of the modeling results did not improve as expected. Therefore, one consider to try another model which use fewer parameters but the correlation of simulation and measurement should not degrade and should be a causal model.

Idea 4 is based on idea 2, $\tan\delta = A(1 - e^{-\alpha\omega})$. By using the combination of Debye and Lorentz model, this model can assure causal, the expression is shown below

$$\varepsilon = \varepsilon_{\text{inf}_d} + \frac{\varepsilon_{s_d} - \varepsilon_{\text{inf}_d}}{1 + j\omega\tau_d} + a * \left(\varepsilon_{\text{inf}_l} + \frac{(\varepsilon_{s_l} + \varepsilon_{\text{inf}_l})\omega_0^2}{\omega_0^2 + j\omega\delta_l - \omega^2} \right) \quad (1-29)$$

where ε is the total permittivity, $\varepsilon_{\text{inf}_d}$ and ε_{s_d} is the relative permittivity value of the Debye model at infinity time and DC, respectively. τ_d is the relaxation for Debye model. A is the number of Lorentz model, $\varepsilon_{\text{inf}_l}$ and ε_{s_l} is the relative permittivity value of Lorentz term at infinity time and DC. Equation 1-29 is a casual model and the $\tan\delta$ has the similar trend as exponential equation used in Ideal 2. But this ideal includes too many parameters, it is difficult to tune the extraction set with so many parameters. Therefore, the equation needs to reduce the parameters. Equation (1-29) also can be expressed as

$$\varepsilon = \varepsilon_d + \sum \varepsilon_l \quad (1-30a)$$

the Debye term can be expressed as

$$\varepsilon_d = \varepsilon_\infty + \frac{\Delta\varepsilon_d}{1 + j\omega_d\tau} \quad (1-30b)$$

and the Lorentz term can be expressed as

$$\varepsilon_l = \frac{\Delta\varepsilon_l\omega_0^2}{\omega_0^2 + j\omega\delta - \omega^2} \quad (1-30c)$$

From Equation (1-30a) and (1-30b) the maximum imaginary part frequency is

$$\omega_d = \sqrt{\omega^2 - \left(\frac{\delta}{2}\right)^2} \quad (1-30d)$$

From (1-30), the goal curve which only includes two parameters, $\tan\delta_s$ and f_s , can be obtained and is shown in Equation (1-31)

$$\tan\delta_s = \frac{\Delta\varepsilon_d}{2\varepsilon_{\infty} + \Delta\varepsilon_d} \quad (1-31a)$$

$$f_s = \frac{1}{\tau} \quad (1-31b)$$

In Figure 2.21 an example is shown how the $\tan\delta_s$ and f_s define the $\tan\delta$ curve,

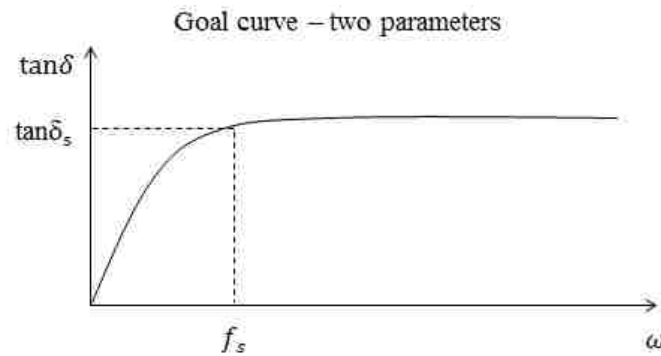
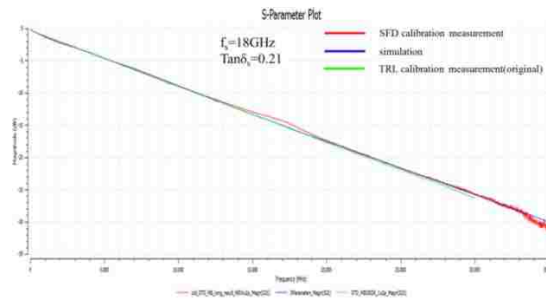


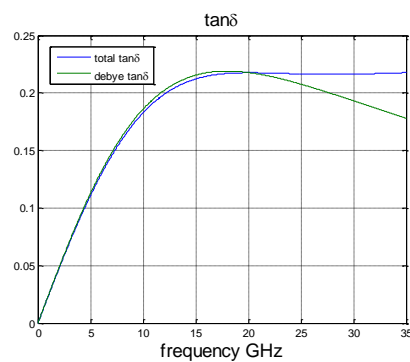
Figure 2.21 $\tan\delta_s$ and f_s illustration plot example

In Figure 2.22(a), it shows old Megtron 6 STD 13mil trace width PCB board measurement and model simulation results. There are three curves shown in the plot, red is the measurement curve using SFD extraction method, green is the measurement result using the TRL extraction method and blue is the model simulation results. The simulation correlated with measurement results very well. Figure 2.22(b) is the tangent loss plot for the additional layer dielectric with the new dielectric model; it maintains the loss at high frequencies but keeps the low frequencies loss the same (compared with the Debye model where loss decreased at high frequencies). Figure 2.22(c) is the comparison plot between additional layer dielectric permittivity Debye model and idea 4 dielectric model. This new model keeps the real part of dielectric permittivity similar compared with first order

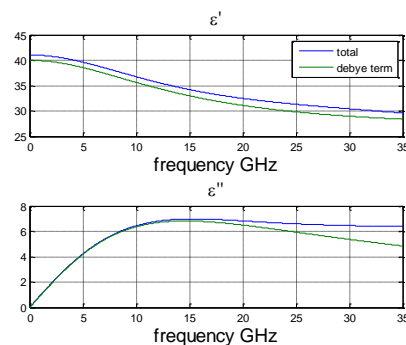
Debye model. For the imaginary part of the dielectric permittivity, compared with traditional Debye model, it does not decrease as rapidly as the Debye model, almost keeps flat at high frequencies.



(a)



(b)



(c)

Figure 2.22 Old Megtron6 STD 13mil trace width board (a) SFD measurement, TRL measurement, and simulation results plot. (b) additional dielectric layer tangent loss curve plot. (c) additional layer dielectric permittivity curve plot

This idea also fits for all 12 boards, Megtron6 MB with three different foil types (STD, VLP/RTF, HVLP) and four trace widths (3.5mil, 9.5mil, 13mil, 15mil). Table 2.3 shows all the parameters used for the new dielectric layer tangent loss calculation.

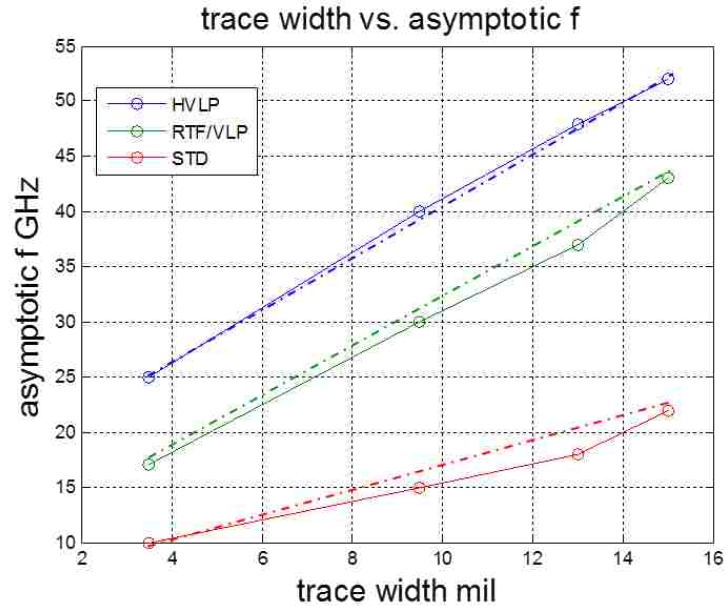
Table 2.3 Summary of the parameters which for 12 boards modeling use idea 4

(MB)	3.5	9.5	13	15
HVLP	f=25GHZ Tan δ =0.142	f=40GHZ tan δ =0.43	f=48GHZ tan δ =0.33	f=52GHZ Tan δ =0.56
VLP/RTF	f=17GHZ tan δ =0.097 RTF	f=30GHZ Tan δ =0.075 RTF	f=37GHZ tan δ =0.19 VLP	f=43GHZ tan δ =0.33 RTF
STD	f=10GHZ tan δ =0.038	f=15GHZ tan δ =0.048	f=18GHZ tan δ =0.21	f=22GHZ tan δ =0.2

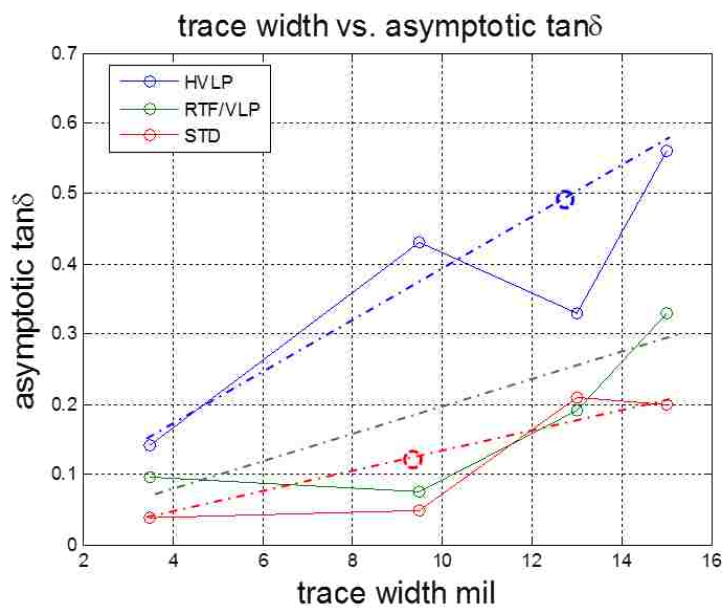
This dielectric model can be fitted with a linear trend, it is shown in Figure 2.23; this is the intuitive design curve plot for method II. For $\tan\delta_s$ the linear trend is not as good as f_s .

In this section, shows the surface roughness represents the additional dielectric layer can be used to model the low-loss and low surface roughness transmission line process. This method begins with first order Debye model, then tried three other models. From the different dielectric model, the requirements for the dielectric model become clear; this model should be a casual model and $\tan\delta$ should not decrease at high frequencies. There should be fewer parameters in the model, otherwise, it is difficult to find the trend that can be used for later. After three tries, ideal 4 actually provide very good results. However, this method did not continue as the project going on. The main

reason is that the company wants to use ADS to run this method and this model requires using 2D cross-section analysis.



(a)



(b)

Figure 2.23 (a) f_s vs trace width plot with linear fitted trend (b) $\tan\delta_s$ vs. trace width plot with linear fitted trend

Method II – Add Dispersive Dielectric Term. This method focuses on representing the surface roughness using the dispersive dielectric term. The diagram of the surface roughness modeling algorithm is shown in Figure 2.24

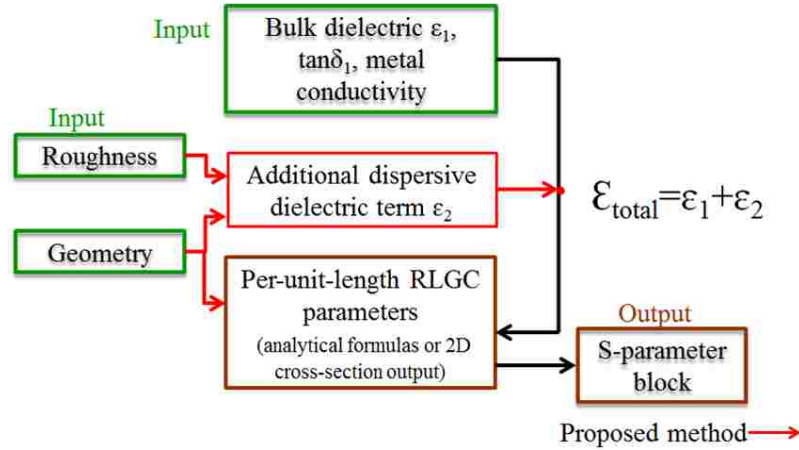


Figure 2.24 Proposed surface roughness modeling algorithm

In an earlier study, a practical causal approximation for low-dispersive dielectrics often used in the PCBs (Djordjevic model) is presented. The dielectric constant was calculated as follows:

$$Re\{\varepsilon_r(\omega)\} = \varepsilon' \approx \varepsilon'_\infty + \frac{\Delta\varepsilon'}{m_2 - m_1} \cdot \frac{\ln(\frac{\omega_2}{\omega})}{\ln(10)} \quad (1-32a)$$

$$Im\{\varepsilon_r(\omega)\} = \varepsilon'' \approx \frac{\Delta\varepsilon'}{m_2 - m_1} \cdot \frac{-\frac{\pi}{2}}{\ln(10)} \quad (1-32b)$$

Besides the dielectric parameters ε'_∞ and $\Delta\varepsilon'$, the model is characterized by two frequency limits $\omega_1 = 10^{m_1}$ and $\omega_2 = 10^{m_2}$. Usually, the lower frequency limit is set to a kHz value and the upper one is set to a THz value. This allows generating the causal dielectric constant function that is practically constant in the frequency range of interest of typical signal integrity simulations (MHz – tens of GHz). Most of the dielectrics used

for PCB manufacturing are indeed very low-dispersive (at least starting from 5-10 GHz) [16 - 22]. However, as was indicated above, the low-loss transmission lines, often exhibit an increase in the slope of the insertion loss (S21) curve with frequency, which cannot be accounted by the existing models.

Although typical PCB dielectrics have low dispersion, it is possible to model the frequency-dependent slope of S21 by adding an effective dispersive dielectric term to the bulk dielectric, accounting for the roughness effect in this manner.

In the proposed model, the bulk dielectric of the transmission line is calculated as $\epsilon_{tot} = \epsilon_1 + \epsilon_2$ (Figure 2.25), where both terms ϵ_1 and ϵ_2 are calculated according to Djordjevic (as shown in Equations 1-27a and 1-27b). The first term is non-dispersive and describes the ‘nominal’ behavior of the dielectric and the second term is dispersive and accounts for the roughness effect.

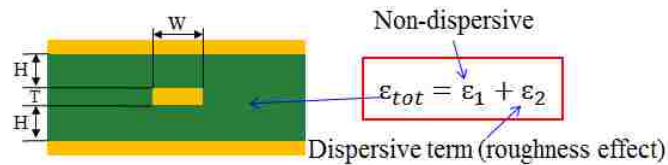


Figure 2.25 Stripline geometry

The parameters of the non-dispersive term ϵ_1 are calculated by specifying the desired values of ϵ' and $\tan\delta$ at a certain frequency, and using the frequency limits ω_1 and ω_2 in the kHz and THz frequency range correspondingly.

A similar procedure is applied to calculate the dispersive part ϵ_2 with the following exceptions: the ϵ'_2 is set such that $\epsilon'_2 \ll \epsilon'_1$ (in the examples below, ϵ'_2 is set to 0.1 for $\epsilon'_1 \approx 4$); the lower frequency limit $\omega_1 = 2\pi f_s$ is set in the GHz frequency range;

and $\tan\delta_s$ is specified at the lower frequency limit. The two parameters of the dispersive term ($\tan\delta_s$ and f_s) are illustrated in Figure 2.21.

The non-dispersive term had nominal values of DK and DF of 3.8 and 0.006 respectively. The lower frequency limit for the non-dispersive term is 10 kHz and the upper one is 1 THz. For the dispersive term $\tan\delta_s = 0.12$ and $f_s = 9$ GHz. As shown in Figure 2.26, the proposed method allows generating the causal permittivity function that has the almost frequency independent real part (DK) and at the same time frequency dependent loss tangent ($\tan\delta$), the parameters of which can be set independently of DK.

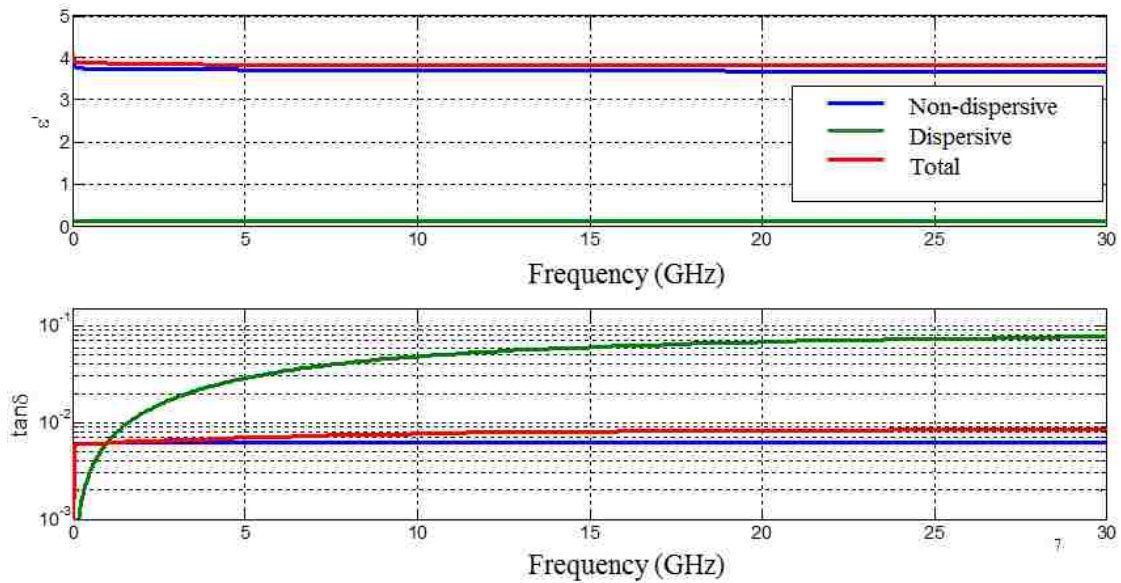


Figure 2.26 Bulk dielectric modeling example

After the permittivity function is generated, the transmission coefficient of the stripline is calculated analytically based on an earlier study [23 - 24].

The proposed model requires two parameters: f_s and $\tan\delta_s$, both of which depend on the roughness and the geometry of the stripline. These parameters are determined

empirically. This method uses the same extraction set as illustrated in the method I. For each TV, a model was built as described above, using known values for the bulk dielectric permittivity ($\epsilon_1' = 3.8$) and loss tangent ($\tan \delta = 0.006$).

The parameters of the dispersive layer f_s and $\tan \delta_s$ were tuned for each case to ensure the best match between the measured and calculated transmission coefficients. The transmission coefficient curves along with the tuned parameters are shown in Figure 2.27.

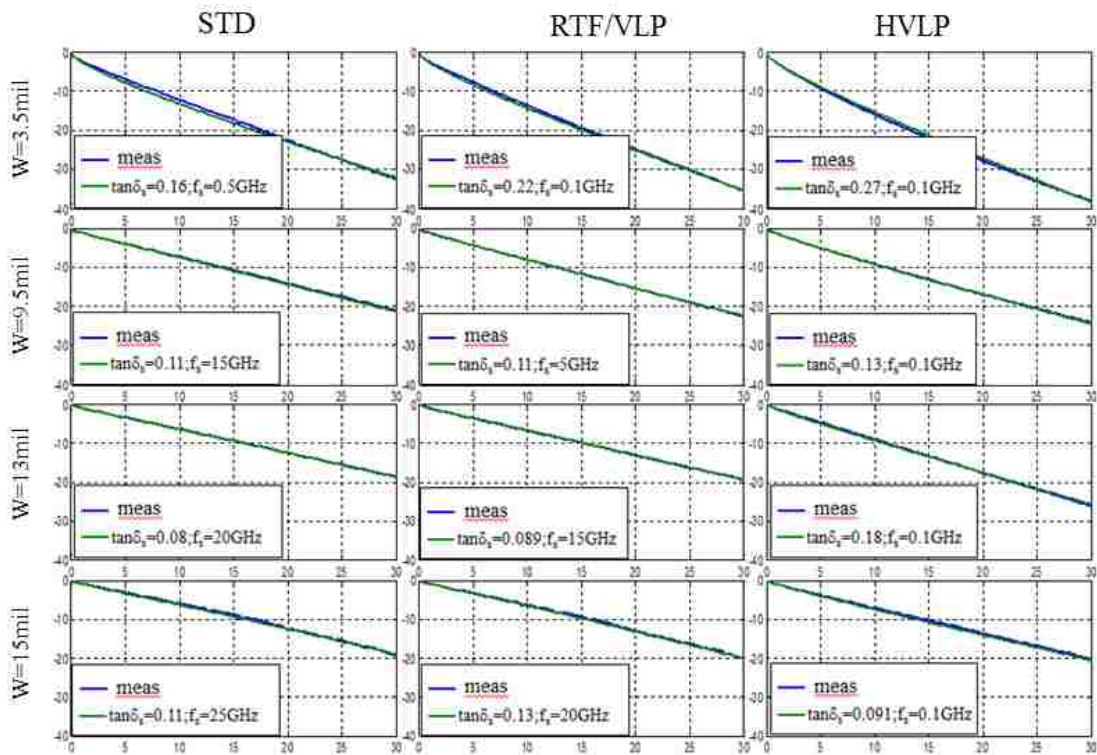


Figure 2.27 Complete $|S_{21}|$ in dB vs frequency in GHz for the entire TV set

The extracted parameters of the dispersive term are shown in Figure 2.28, along with the linearly fitted approximation (design curves). The obtained design curves allow determining the dispersive term parameters for arbitrary line width, provided that the

roughness of the modeled transmission-line resembles one of the roughness grades (STD, RTF/VLP, HVLP) used for the parameter extraction.

The design curves were extracted for the Megtron 6 dielectric material. However, these can be extended to be used for other low-loss materials, using the following normalization scheme:

$$\tan\delta_{s_other} = \frac{\tan\delta_{0_other}}{\tan\delta_{0_meg6}} \tan\delta_{s_meg6} \quad (1-33)$$

where $\tan\delta_{s_meg6}$ is the value from design curve for Megtron 6 board, $\tan\delta_{s_other}$ is the other material dispersive term dielectric loss, $\tan\delta_{0_meg6}$ is the loss tangent for the Megtron6 and $\tan\delta_{0_other}$ is the loss tangent for the other material.

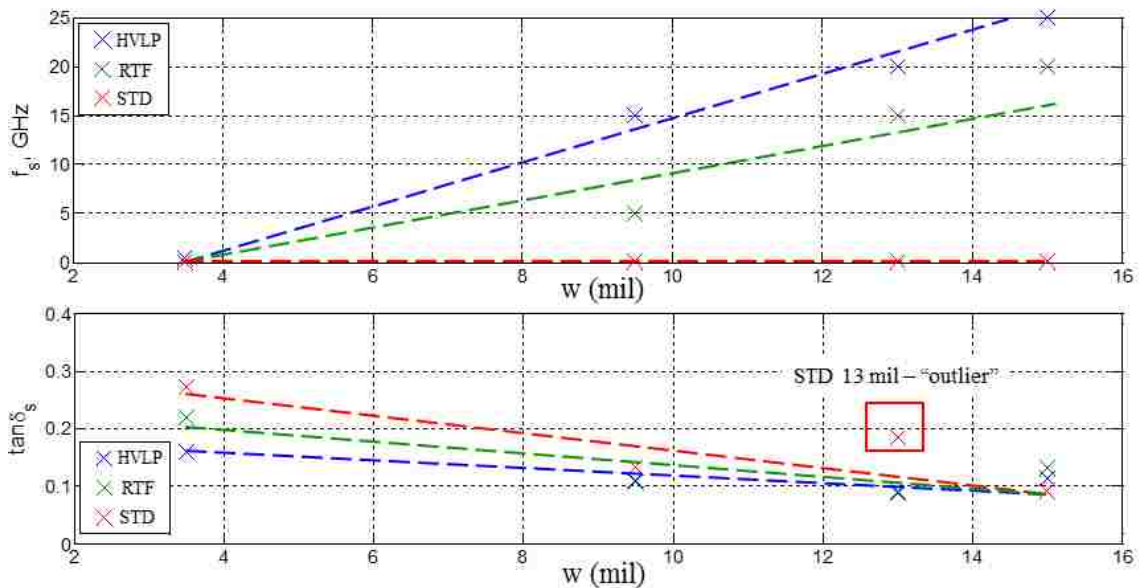


Figure 2.28 Design curves for the surface roughness behavioral model (dispersive dielectric parameters) as a function of trace width

For this study, fourteen cases were used to validate the behavioral model. As shown in Figure 2.29, the validation set includes high-loss and middle-loss materials

($\tan\delta > 0.01$) as well as low-loss material ($\tan\delta \leq 0.008$), with different trace widths and roughness.

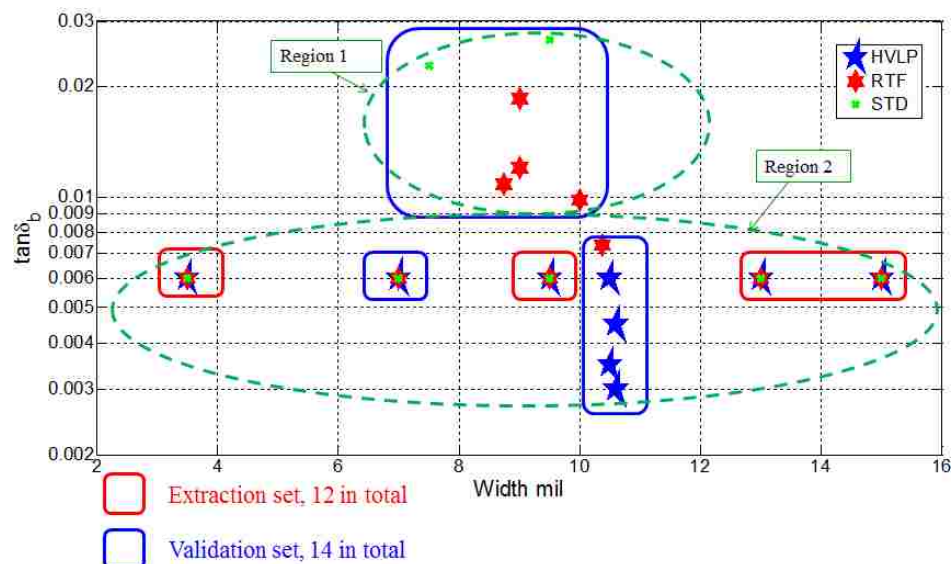


Figure 2.29 Available boards map--extraction and validation boards

Figure 2.30 to 2.34 show five examples of the validation of the behavioral model compared with the results obtained in ADS. Each example has a different trace width, material, and roughness.

As can be observed, there is no need to use behavioral model for high and middle-loss dielectrics marked as 'region 1' in Figure 2.29 (the same is true for ADS model, as the inclusion of roughness in that model also leads to substantial overestimation of loss – see green lines in Figure 2.33 and Figure 2.34). However, for the low-loss materials (region 2), the behavioral model improves the modeling accuracy. The impulse response accuracy is also improved compared to the roughness modeling implemented in ADS. The reason for the differences in the behavior of low- and middle-loss boards with regard to roughness is under investigation.

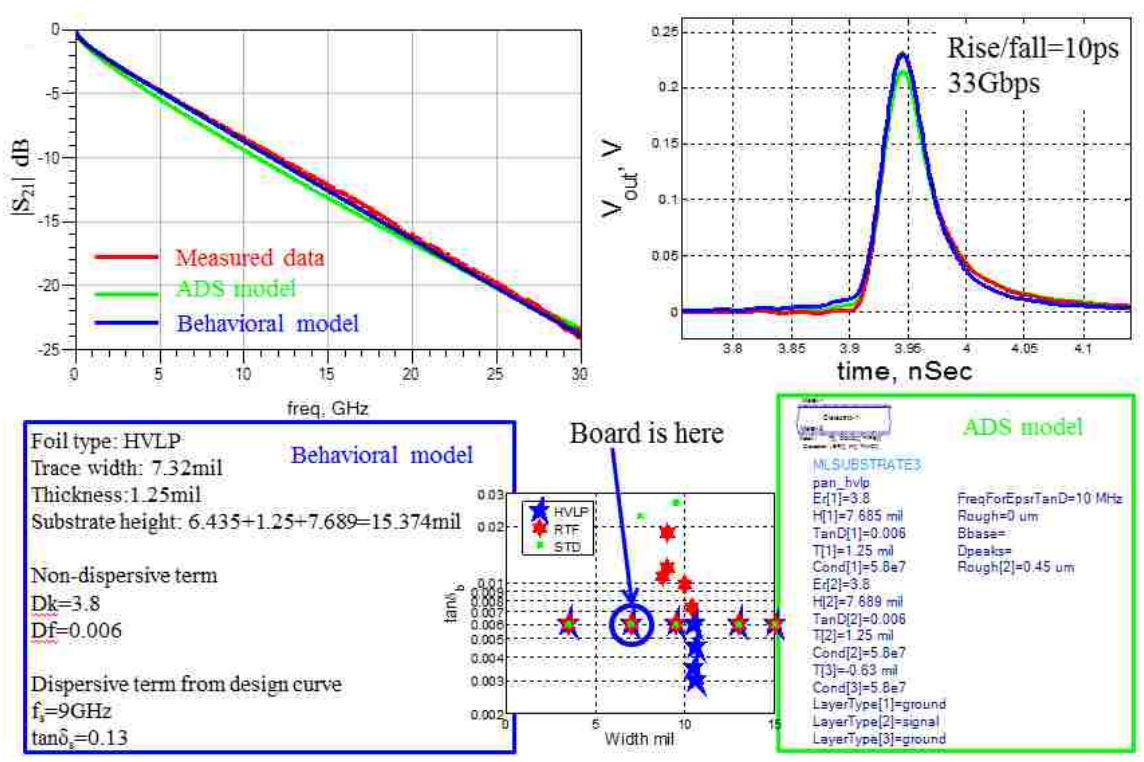


Figure 2.30 Simulation results for Megtron6, HVLP foil, 7.32mil trace width

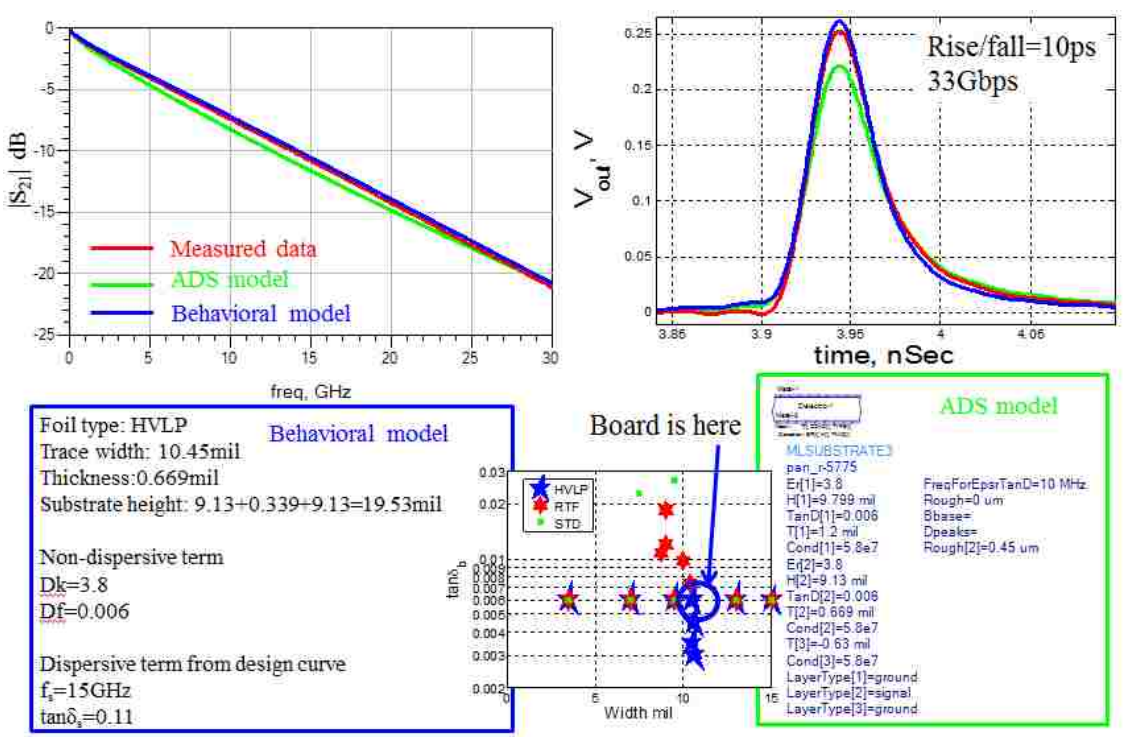


Figure 2.31 Simulation results for Megtron6, HVLP foil, 10.45mil trace width

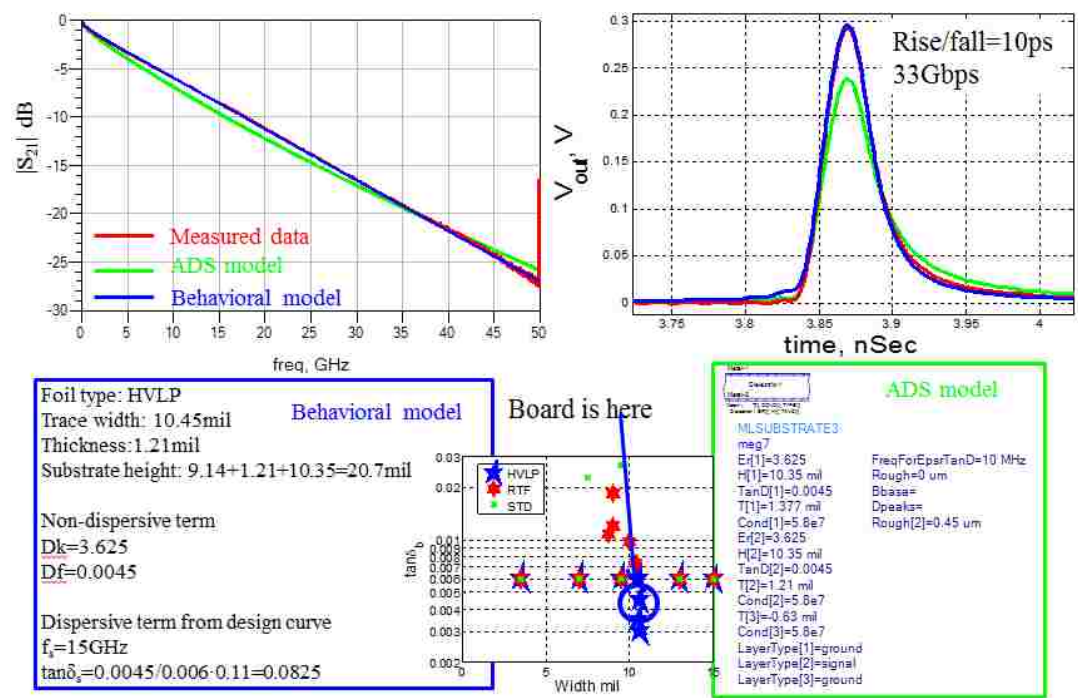


Figure 2.32 Simulation results for Megtron7, HVLP foil, 10.45mil trace width

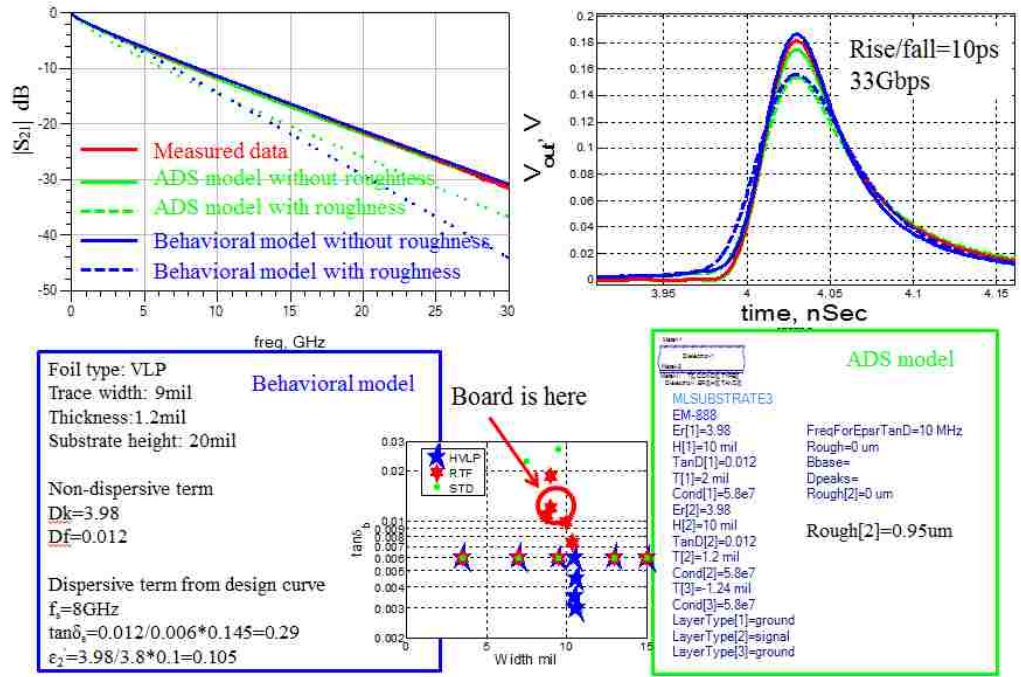


Figure 2.33 Simulation results for middle-loss material, VLP foil, 9mil trace width

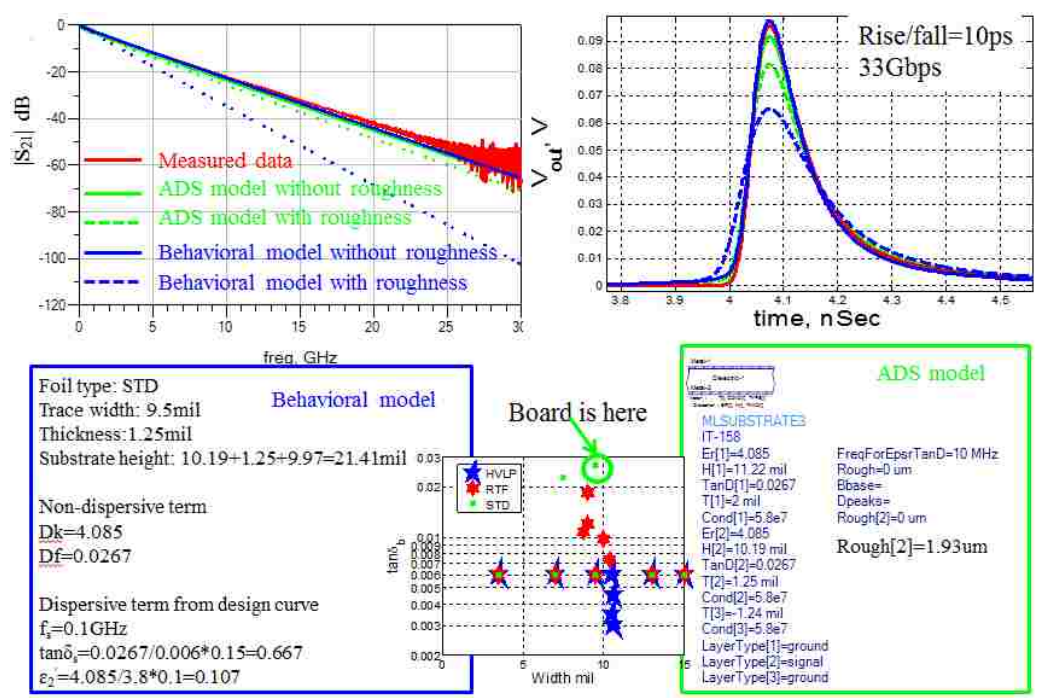


Figure 2.34 Simulation results for high-loss material, STD foil, 9.5mil trace width

3. HIGH-SPEED TEST BOARD VIA-TRANSITION OPTIMIZATION

3.1. BACKGROUND

With the demanding on high bandwidth transition, the impedance discontinuity in the channel is stricter. Usually, via-transition is the main reason, which causes the discontinuity, cause extra inductance or capacitance depends on how the transition part designed. 2D and full-wave 3D simulation solver are been used to analyze the impedance signature in this section. Single-ended trace impedance should be 50Ω and differential trace impedance should be 100Ω . Additional, at 50GHz, insertion loss should as flat as possible close to 0dB and return loss should as low as possible, expect to be lower than 10dB.

The optimization is based on previous CISCO test board design. The first reason for this optimization is to change the ground via signature. Figure 3.1 shows that aperiodic spacing of the ground via wall along the test trace, which reduces undesirable resonances due to the proximity of ground via wall structure to the signal trace. However, the ground via wall is even on the two sides of the signal trace, so the signal still has some effect.

Second is to optimize this design is to improve the insertion loss and reduce the return loss. Figure 3.2 shows the time-domain (TDR) and frequency-domain (S-parameter) results from the last version. From the simulation results, this design will perform well until 47 or 48GHz. At 50GHz, return loss is approximate -2dB; it may affect the signal high-frequency performance.

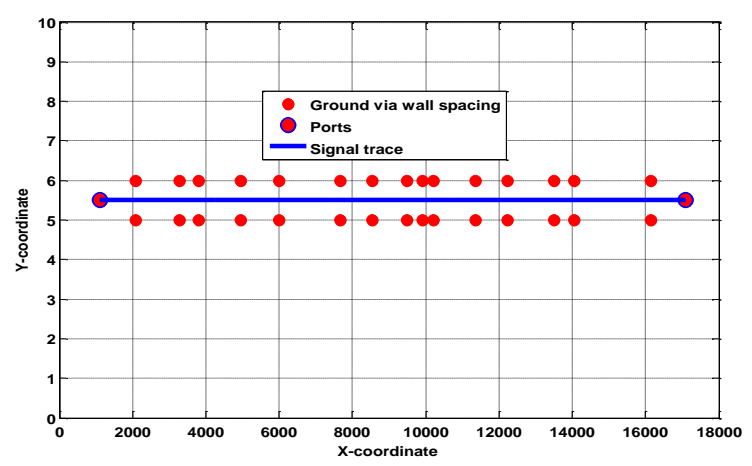


Figure 3.1 Example of distribution of the 15 ground via columns along the test trace

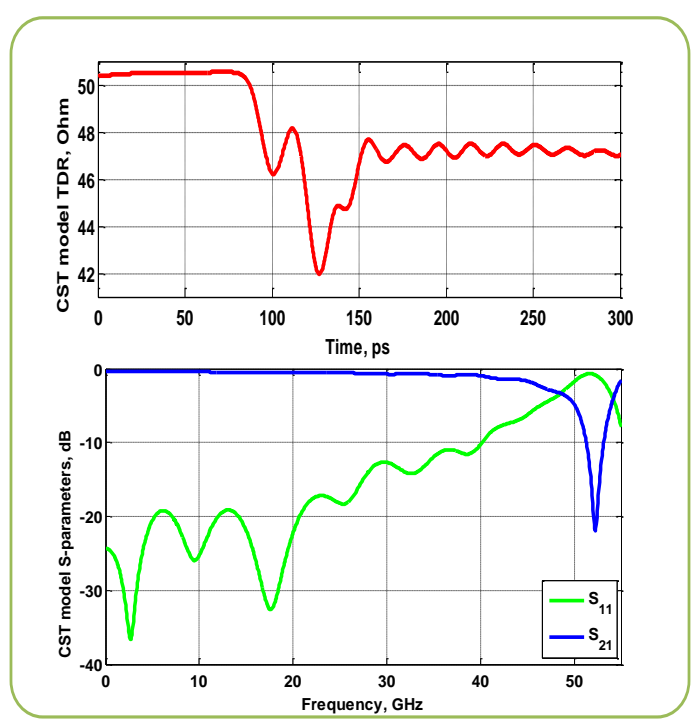


Figure 3.2 Achieved S-parameters and TDR

Last design has 3D full wave model and cadence allegro file. In Figure 3.3, it shows the allegro drawing from last design; in this version, it uses TRL calibration pattern. The single-ended and the differential signal trace length is 16inch (16,025mil).

For single-ended, the trace characteristic impedance from top to bottom is 48Ω , 50Ω and 52Ω and trace width is 9.8mil, 9mil, and 8.2mil. For differential trace, the trace impedance from top to bottom is 96Ω , 100Ω and 104Ω ; trace pitch is the same, all of them are 15mil and trace width is 8.8mil, 8.1mil, and 7.4mil. In the new version, use SFD calibration pattern to replace TRL pattern. In the new version, only consider 50Ω and 100Ω for single-ended and differential, respectively.

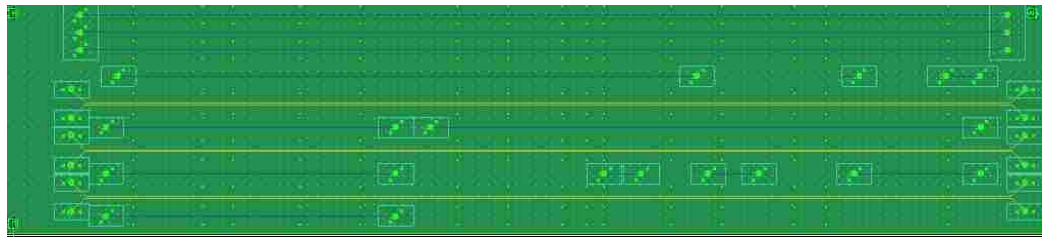


Figure 3.3 Allegro PCB design drawing from the last version

In the new version, expect three different modifications. First, the ground via wall pattern, second the S-parameter improvement and third SFD calibration pattern and different trace length.

3.2. VERSION I

In this part will show the first version modification from last design. Version 1 test board design uses MEGTRON7 Lineup material low-Dk glass, the laminate is R-5785(N) and prepreg is R-5680(N). The designed stackup shows in Figure 3.4.

Based on the stackup, the 2D cross-section and 3D full wave modeling built for analysis. Figure 3.5-3.6 shows the 2D cross-section model and simulation results for both single-ended and differential cases.

		DK	Thickness
1			2.4
	1035 77%	3.2	3.9
2			0.6
	2x1035 72%	3.14	4.72
3			0.6
	1035 77%	3.2	3.9
4			0.6
	2x1078 72%	3.08	9.28
5			0.6
	1035 77%	3.2	3.9
6			0.6
	2x1035 72%	3.14	4.72
7			0.6
	1035 77%	3.2	3.9
8			2.4

Figure 3.4 Desired PCB stackup design

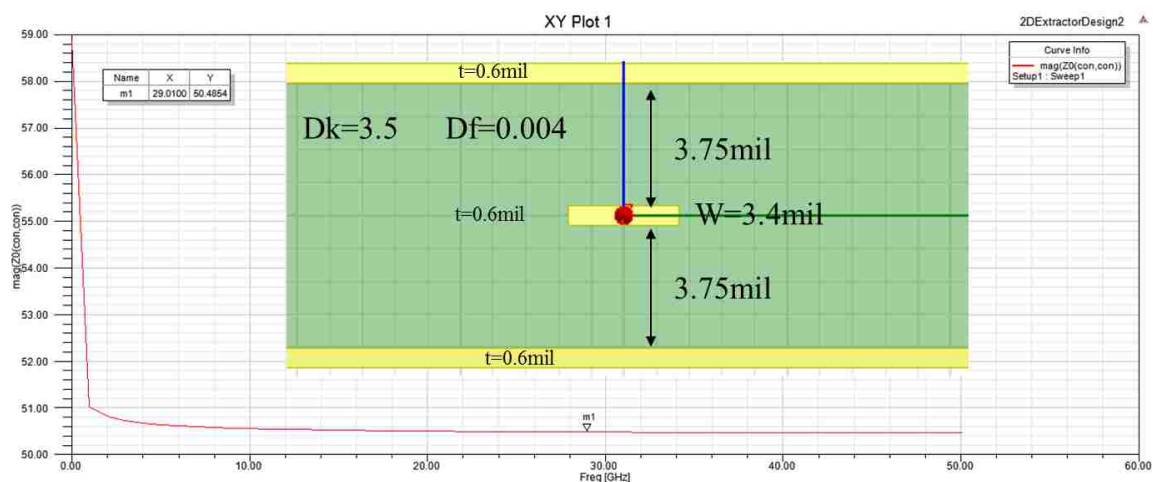


Figure 3.5 Single-ended 2D cross-section analysis results

After has the 2D modeling results, the cross-section and stackup are determined, therefore, has enough information to build 3D full wave model. However, as Figure 3.4 shows that, at that point didn't notice the DK and DF was different from dielectric vendor suggest, all the DK and DF used in the simulation is 3.5 and 0.004 respectively. This should not affect the trace impedance significantly, since the PCB shop will adjust the

trace width based on the real situation, but will have some minor effects for the via-transition part since this will affect the antipad size.

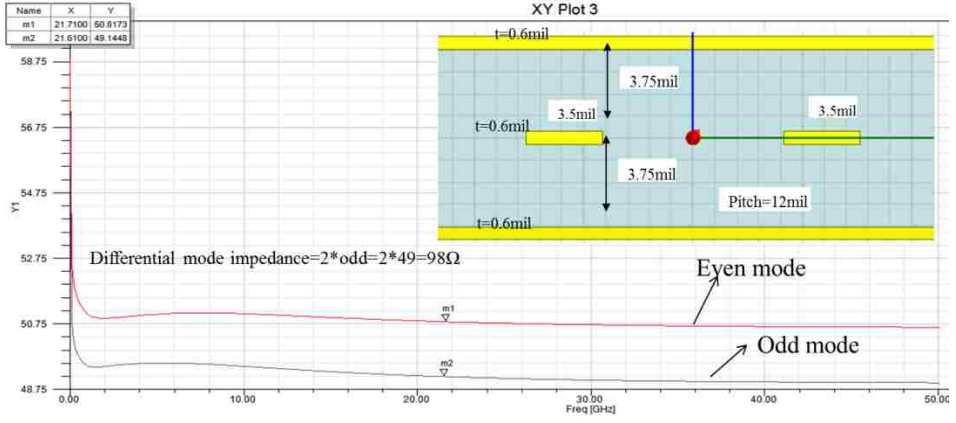


Figure 3.6 Differential 2D cross-section analysis results

First built the 3D model for the single-ended case, analyze the results in the time and frequency domain to decide the via-transition structure. There several key elements designing the via-transition, via, pad, anti-pad and diving board size. All these elements will make sure the transition close to 50Ω and reduce the impedance discontinuity. Figure 3.7 illustrate the via-transition key elements.

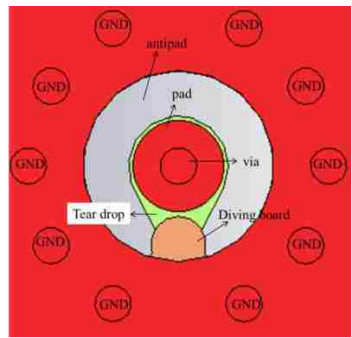


Figure 3.7 Screen shot for via-transition key elements illustration

In order to have a better understanding of the design flow, here will introduce two concepts. First is diving board. This is designed by EMC lab and CISCO. The diving board structure developed to compensate the parasitic inductance, it is the additional part come out from both ground planes adjacent to the trace layer, shows in Figure 3.7 orange part [27]. Second is teardrop. In printed circuit board, a teardrop is typically drop-shaped featured at the junction of via or contact pad and trace. It helps the structural integrity in the presence of thermal or mechanical stresses [28].

To begin the design, first need to design a 50Ω through-hole via structure. Then add the via-to-trace transition. Below is the final 3D model for single-ended simulation. In the model, it removed all the un-functional pads in order to simple PCB manufacture process.

In Figure 3.8, it shows the basic model that will be used. Three models were simulated: with same size diving board, with different size diving board and without diving board. The S-parameters results show in Figure 3.9. The optimized results are better than the last version, especially with the same size diving board case, which shows in Figure 3.2, insertion loss has 2dB improvement and return loss has 3dB improvement at 50GHz.

After analyzing the frequency domain results, time domain also been investigated, as shown in Figure 3.10. From the time domain analysis, TDR results, with the same size diving board will cause the largest extra capacitance compare with the other two cases, but pull down the extra parasitic inductance at the transition and give better frequency domain performance. Therefore, in the real board drawing will use this structure. The same structure will also apply to the differential case.

Single-ended model

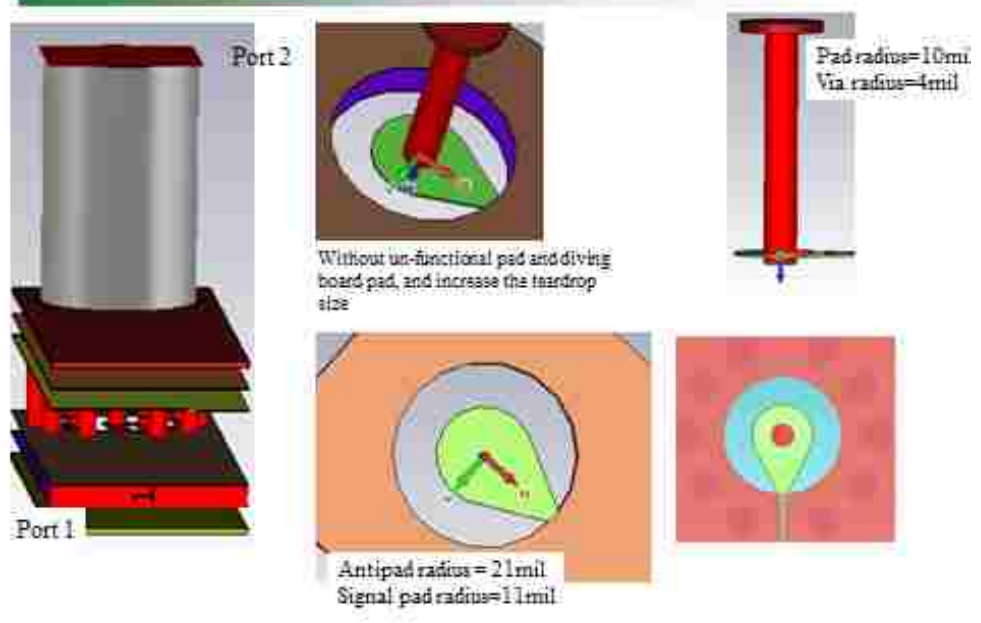


Figure 3.8 Single-ended trace CST model

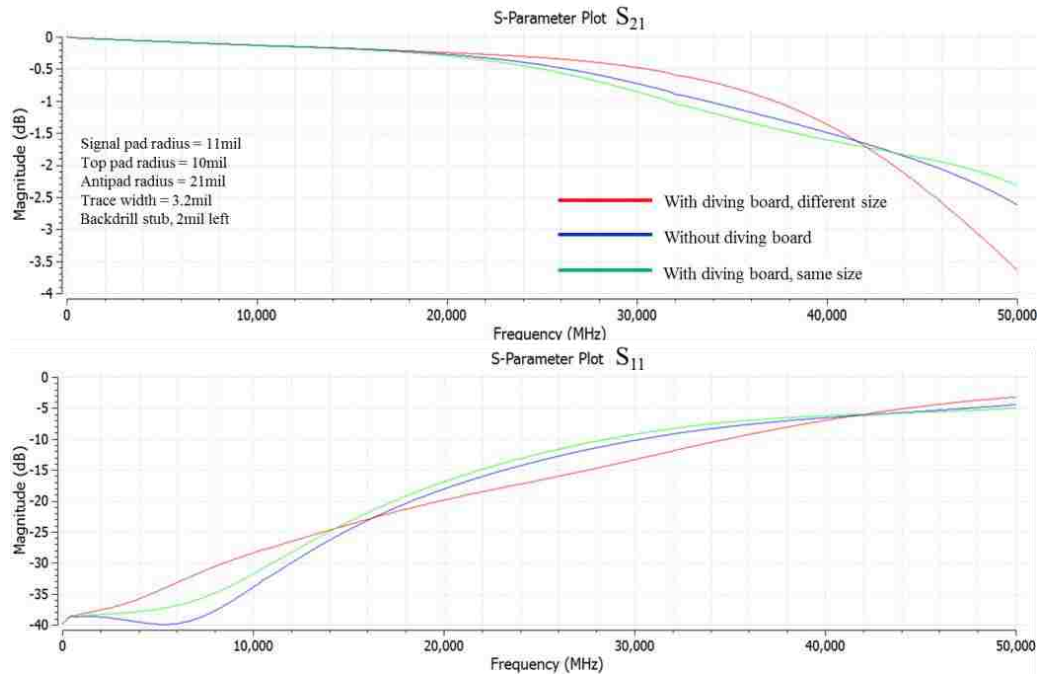


Figure 3.9 Optimized via-transition structure insertion and return loss summary

For differential case, need to consider the two connectors separation. This test board will use 2.4mm JACL 2 HOLE FL MT connector from SV Microwave, Inc. Therefore, differential trace connector center-to-center separation is 499.5mil in order to have enough space for connector installation.

For differential trace, need to do simulation for transition trace part, which from via to normalized trace. The angle α for the transition trace to normalized trace should be 45° . Due to transition trace separation is larger than normalized trace, therefore in order to maintain 100Ω impedance, the transition trace width should be narrower. In Figure 3.11 shows that in the final design, decided to use 3.2mil trace width for transition trace and 3.45mil trace width for normalized trace width. Figure 3.12 and 3.13 shows the frequency domain and time simulation results. As single-ended case, the simulation also has the same cases, with and without diving board cases, but has additional case, which adjusts the transition trace width. Same as single-ended results, with the same size diving board and transition trace width is 3.2mil has the best performance at 50GHz.

After deciding single-ended and differential trace structure, need to implement the structure into cadence allegro then generate the PCB file for manufacture. Figure 3.14 shows the final layout. In the final design, instead of using TRL only use SFD method. SFD only require two different lengths of the trace for de-embedding, one is thru and another is test line. Therefore, for single-ended and differential trace need a 500mil thru line, and 5inch, 10inch, and 16inch test line.

TDR results

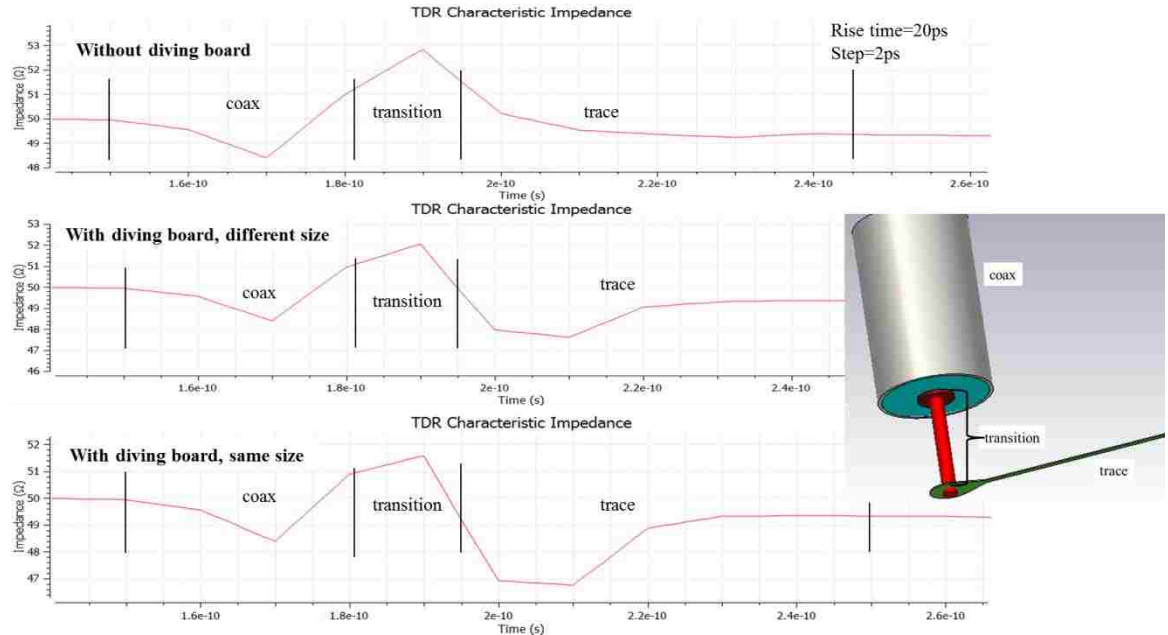


Figure 3.10 Optimized via-transition structure TDR results summary

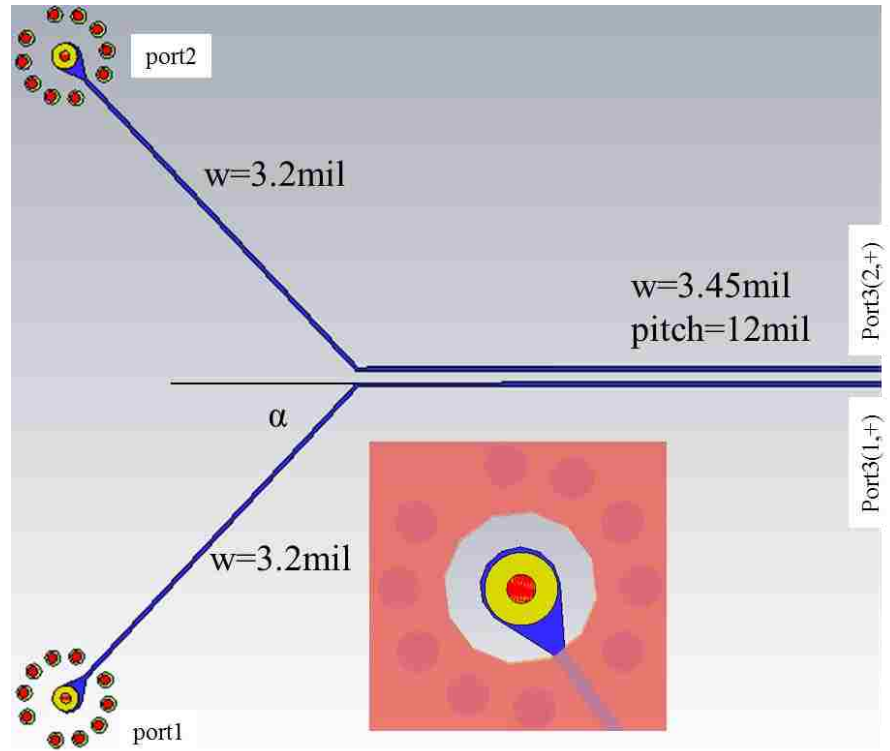


Figure 3.11 Differential trace model in CST

S-parameter results

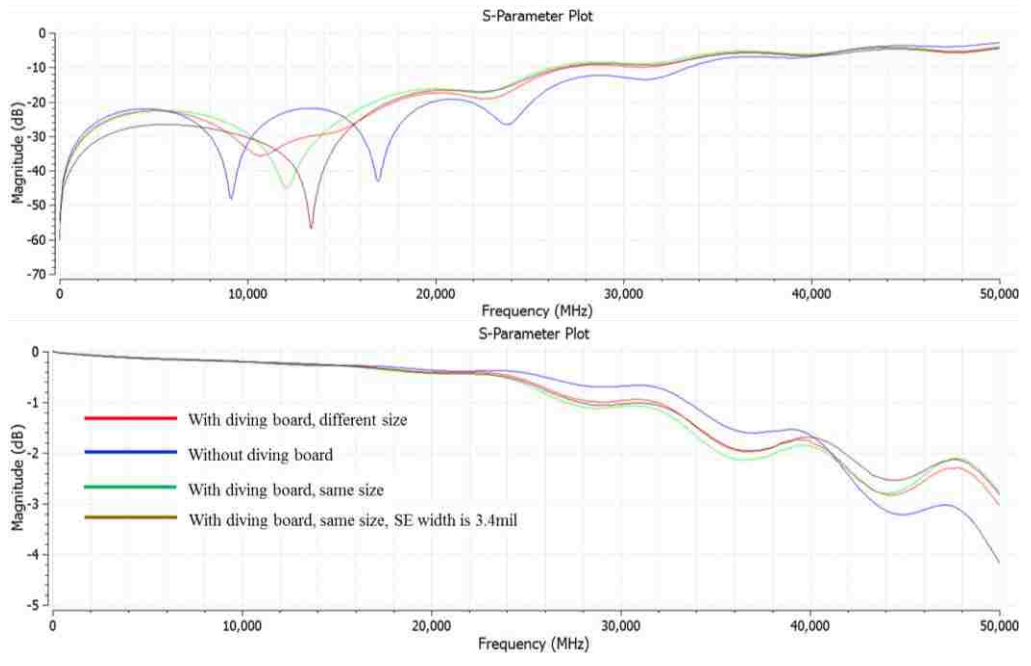


Figure 3.12 Optimized differential via-transition structure insertion and return loss summary

Simulation results - TDR

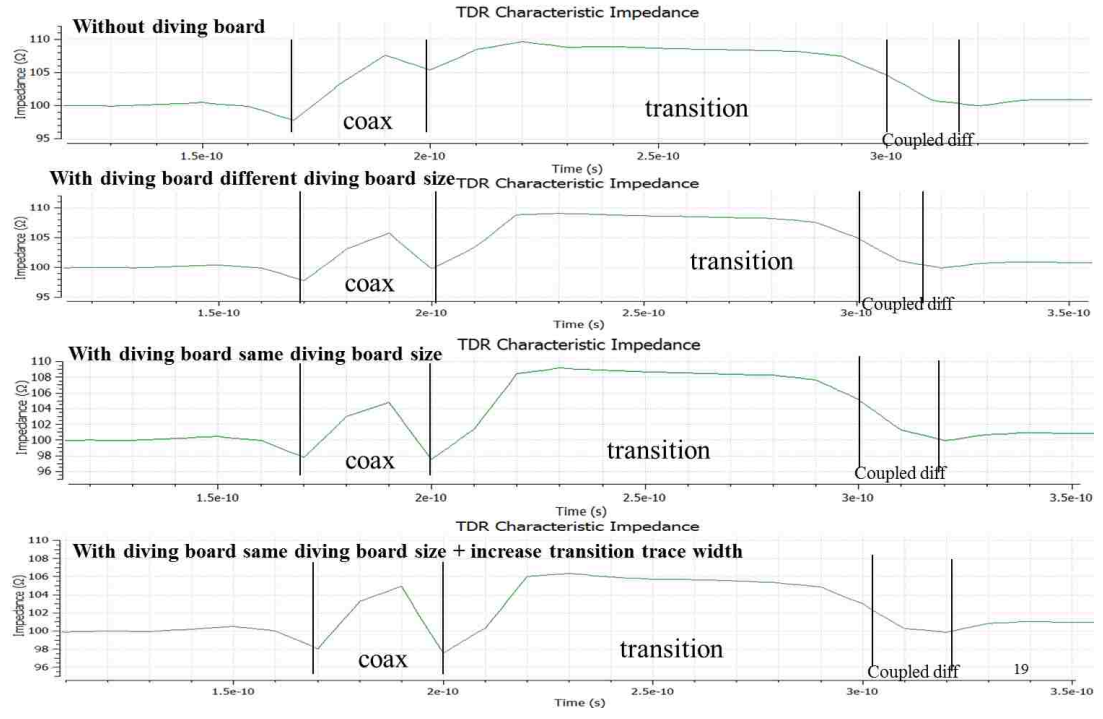


Figure 3.13 Optimized differential via-transition structure TDR results summary

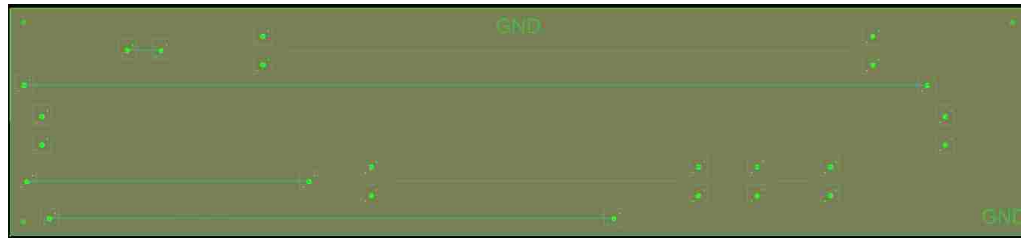


Figure 3.14 Optimized test board layout in cadence allegro

3.3. VERSION II

This section will present another optimized PCB structure design. Version II test board also plan to use MEGTRON7 Lineup material low-Dk glass, the laminate is R-5785(N) and prepreg is R-5680(N). The designed stackup shows in Figure 3.15.

			DK	Thickness
1				2.4
		1035 77%	3.09	2.9
2				0.7
		1035 67%	3.2	3.9
3				0.7
		1035 77%	3.09	2.9
4				0.7
		2116 55%	3.34	9.8
5				0.7
		1035 77%	3.09	2.9
6				0.7
		1035 67%	3.2	3.9
7				0.7
		1035 77%	3.09	2.9
8				2.4

Figure 3.15 Version II test board stackup

Based on designed stackup, 2D cross-section model was built to calculate the characteristic impedance for single-ended and differential cases. In Figure 3.16 and 3.17 shows single-ended and differential impedance, respectively.

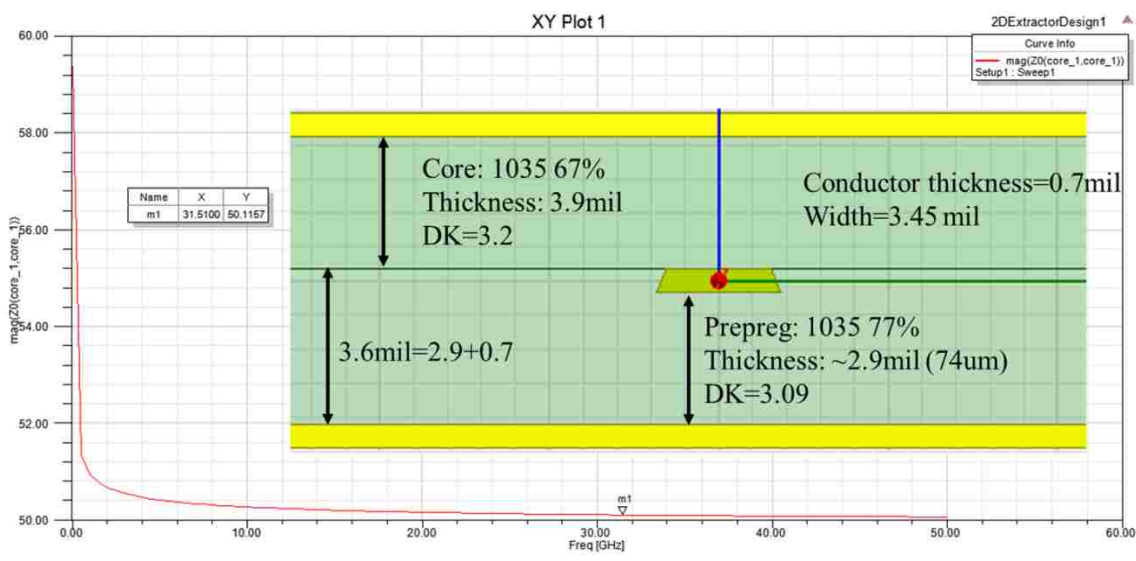


Figure 3.16 2D cross-section analysis for single-ended case

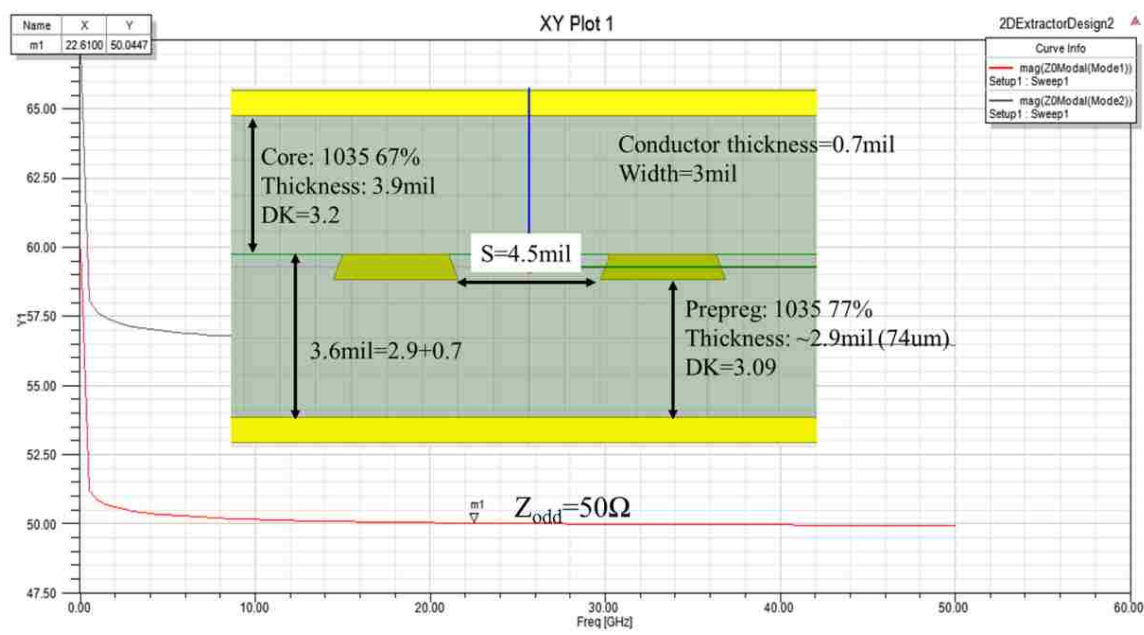


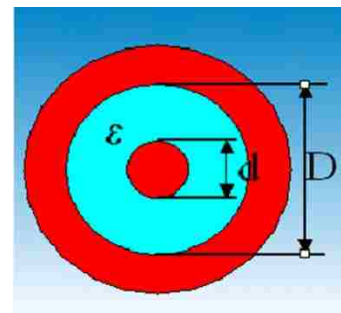
Figure 3.17 2D cross-section analysis for differential case

For this version test board, the trace width and characteristic impedance value requirement for single-ended are 3.5mil and 50 Ω ; the differential case is 3.5mil width and spacing is 3.5-4.5mil, the differential mode impedance should be 100 Ω . According to the 2D cross-section analysis results, the stackup choice meets the requirements, both cases are close to the desired design values.

In Figure 3.18, it shows the PCB stackup. For 3D full wave model starts from the single-ended case, due to deciding the via-transition structure parameters first. The company provides the standard requirement of via, signal pad, antipad size (diameter), they are 7.9mil drill, 17.1mil, and 26mil, need to tune antipad size to reach 50 Ω . The worst backdrill stub length is 12mil and the best backdrill stub length is 2mil. From Table 3.1, both via-transition cases are close to 50 Ω , need to do additional analysis of frequency domain and time domain results to decide the final size, due to the ϵ listed in the table is an estimated value.

Table 3.1 Via-transition and coaxial port impedance list

Coax	d (mil)	D (mil)	ϵ	Z_0 (Ω)
Via-transition 1	8	36	3.2	50.42
Via-transition 2	8	38	3.2	52.23



In Figure 3.19, shows that via-transition 1, with smaller antipad size, will have better insertion and return loss performance, especially for return loss, at least two 2dB different at 50GHz; for insertion loss, no significant improvement, approximate 0.2dB

difference. From frequency-domain analysis results, the via-transition1 case is a little bit better than via-transition 2.

TDR comparison between these two cases shows in Figure 3.20, apparently via-transition2 transition structure is better than via-transition1. Via-transition2 case the antipad size (38mil) is larger than via-transition1 (36mil). As mentioned, $\epsilon=3.2$ is an approximation value, in real cases, the effective ϵ should be less than 3.2 due to prepreg ϵ is 3.09 and also the backdrill fill is air ($\epsilon=1$). Therefore, larger antipad size will provide larger impedance, as expected the transition should be smoother.

Single-ended model

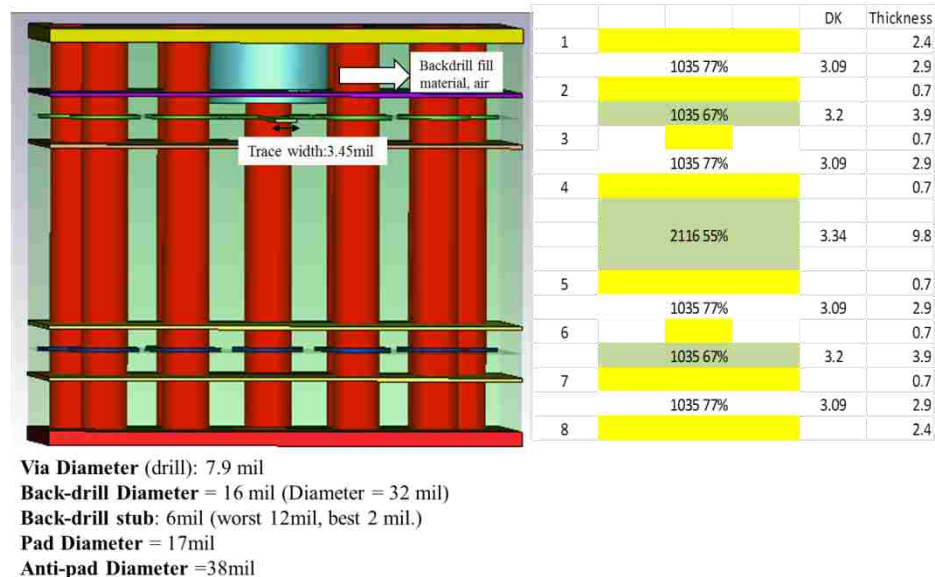


Figure 3.18 Single-ended CST model

Summarize the frequency-domain and time-domain analysis results, decide to use the larger antipad size structure, which is the via-transition2 case. Due to via-transition1 frequency-domain performance is not significantly better but TDR is significantly worse than via-transition2. As showing the figure, all the un-functional pads are removed and

no diving board adds to this design, cause no need to compensate extra parasitic inductance, if adding the diving board will cause additional parasitic capacitance.

Differential trace will have the same via-transition structure. The 3D full wave modeling will simulate the transition trace width.

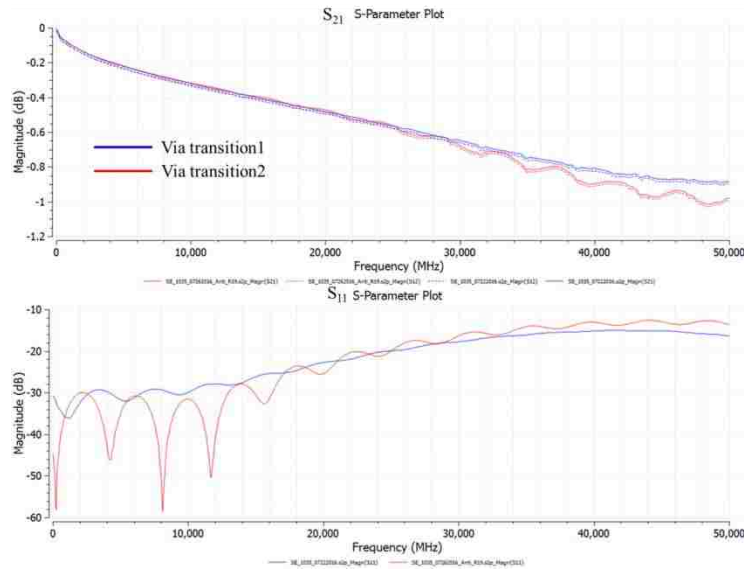


Figure 3.19 Insertion and return loss for different via-transition size

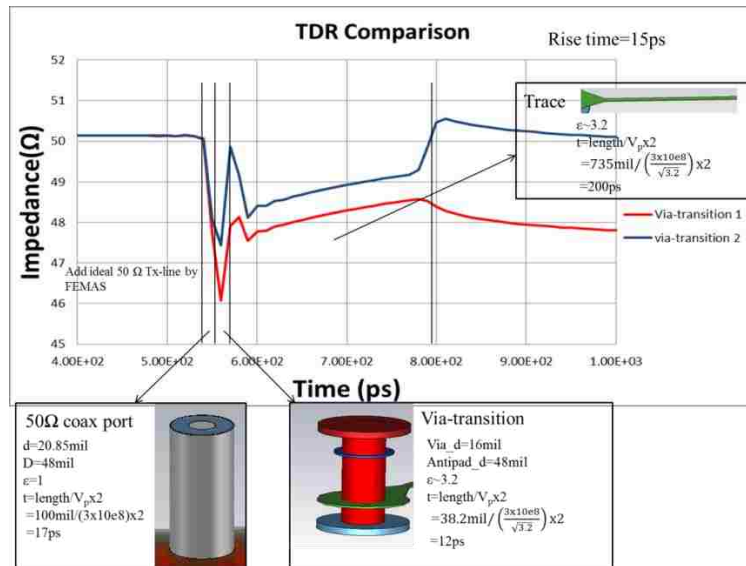


Figure 3.20 Time-domain results for different via-transition size

4. CONCLUSION

In Section 2.1 shows how the behavioral model was developed and why decided to add a dispersive dielectric term to build the dielectric model. Fifteen validation cases are provided which indicate that this model has a significant improvement compared with the presented model for low-loss and low surface roughness transmission line. The model is capable of capturing the frequency-dependent $|S_{21}|$ slope and has better agreement with the measurement up to 30GHz. However, this model still not perfect. In the future, another degree of freedom in the design curve needs to be included - foil roughness. The 2D design curve needs to be developed into a 3D design curve which will improve the modeling accuracy. In addition, the physics of conductor surface roughness effect should be investigated to more clearly understand how the foil roughness affects the loss for the low-loss and low surface roughness transmission line at high frequencies. Last, since this behavioral model dielectric permittivity non-dispersive part is highly dependent on the material extraction method how to improve the accuracy of material tangent loss value (not include the foil roughness) needs to be investigated.

In Section 3.1 presents two version PCB optimization results. Both PCB design is better than the original design. From these two PCB design can summarize a high-speed test board design flow for later optimization. First, based on company trace width requirement and dielectric material to run 2D cross-section modeling for rough estimation of stackup. Then correlate the stackup with the real thickness suggest in the vendor manual to run another 2D cross-section evaluation to validate the desired trace width. Then start from the single-ended trace, to decide the via-transition geometry, via, signal pad and antipad size. Also, need to run simulation about the backdrill stub length,

usually this length should base on company suggestion and mechanical restriction. Then decide whether need the diving board or not. After settling these details, then run the differential case to decide the transition trace width in order to have a smooth transition.

BIBLIOGRAPHY

1. Bogatin, Eric. Signal and Power Integrity: Simplified. Upper Sadle River (NJ): Prentice Hall, 2010. Print
2. https://en.wikipedia.org/wiki/Skin_effect
3. Stephen H. Hall, Howard L. Heck. "Advanced Signal Integrity for High – Speed Digital Design" [Online] Available: <http://onlinelibrary.wiley.com/book/10.1002/9780470423899>
4. John David Jackson. Classical Electrodynamics. John Wiley & Sons Ltd. 1962
5. Hall, S.; Pytel, S.G.; Huray, P.G.; Hua, D.; Moonshiram, A.; Brist, G.A.; Sijercic, E., "Multigigahertz Causal Transmission Line Modeling Methodology Using a 3-D Hemispherical Surface Roughness Approach," in Microwave Theory and Techniques, IEEE Transactions on , vol.55, no.12
6. Djordjevic A.R.; Biljic, R.M.; Likar-Smiljanic, V.D.; Sarkar, T.K., "Wideband frequency-domain characterization of FR-4 and time-domain causality," in Electromagnetic Compatibility, IEEE Transactions on , vol.43, no.4, pp.662-667, Nov. 2001 doi: 10.1109/15.97464
7. P. Huray, S. Hall, S. Pytel, F. Oluwafemi, R. Mellitz, D. Hua, and P. Ye, "Fundamentals of a 3-D snowball model for surface roughness power losses," in Signal Propagation on Interconnects, 2007. SPI 2007. IEEE Workshop on, May 2007, pp. 121-124
8. P. G. Huray, O. Oluwafemi, J. Loyer, E. Bogatin, and X. Ye, "Impact of copper surface texture on loss: A model that works," DesignCon 2010 Proceedings, 2010
9. Koul, A.; Koledintseva, M.Y.; Hinaga, S.; Drewniak, J.L., "Differential Extrapolation Method for Separating Dielectric and Rough Conductor Losses in Printed Circuit Boards," in Electromagnetic Compatibility, IEEE Transactions on , vol.54, no.2, pp.421-433, April 2012]
10. Shlepnev, Y.; Nwachukwu, C., "Roughness characterization for interconnect analysis," in Electromagnetic Compatibility (EMC), 2011 IEEE International Symposium on , vol., no., pp.518-523, 14-19 Aug. 2011
11. Xichen Guo; Jackson, D.R.; Koledintseva, M.Y.; Hinaga, S.; Drewniak, J.L.; Ji Chen, "An Analysis of Conductor Surface Roughness Effects on Signal Propagation for Stripline Interconnects," in Electromagnetic Compatibility, IEEE Transactions on , vol.56, no.3, pp.707-714, June

12. S. De, A. Gafarov, M. Y. Koledintseva, R. J. Stanley, J. L. Drewniak and S. Hinaga, "Semi-automatic copper foil surface roughness detection from PCB microsection images," *Electromagnetic Compatibility (EMC), 2012 IEEE International Symposium on*, Pittsburgh, PA, 2012, pp. 132-135
13. A.V. Rakov, S. De, M. Y. Koledintseva, S. Hinaga, J. L. Drewniak and R. J. Stanley, "Quantification of Conductor Surface Roughness Profiles in Printed Circuit Boards," in *IEEE Transactions on Electromagnetic Compatibility*, vol. 57, no. 2, pp. 264-273, April 2015
14. Ippich, "A Design Experiment for the Influence of Copper Foils on Impedance, DC Line Resistance and Insertion Loss," *IPC APEX Expo 2012*
15. Y. Shlepnev, "Dielectric and Conductor Roughness Models Identification for Successful PCB and Packaging Interconnect Design up to 50 GHz," *The PCB Design Magazine* 02/2014; 2014(2):12-28
16. Koledintseva, M.Y.; Razmadze, A.G.; Gafarov, A.Y.; Soumya De; Drewniak, J.L.; Hinaga, S., "PCB conductor surface roughness as a layer with effective material parameters," in *Electromagnetic Compatibility (EMC), 2012 IEEE International Symposium on*, vol., no., pp.138-143, 6-10 Aug. 2012
17. https://en.wikipedia.org/wiki/Effective_medium_approximations
18. <http://ningpan.net/publications/151-200/156.pdf>
19. S. G. Pytel, G. Barnes, D. Hua, A. Moonshiram, G. Brist, R. Mellitz, S. Hall, and P. G. Huray, "Dielectric modeling, characterization, and validation up to 40 GHz," presented at the 11th Signal Propag. on Interconnects Workshop, Genoa, Italy, May 13–16, 2007
20. Deutsch, e.t. "Extraction of $\epsilon_r(f)$ and $\tan\delta(f)$ for Printed Circuit Board Insulators Up to 30 GHz Using the Short-Pulse Propagation Technique," *IEEE Transactions on Advanced Packaging*, vol.28, no.1, Feb. 2005
21. Lei Hua; Bichen Chen; Shuai Jin; Koledintseva, M.; Lim, J.; Qiu, K.; Brooks, R.; Ji Zhang; Shringarpure, K.; Jun Fan, "Characterization of PCB dielectric properties using two striplines on the same board," in *Electromagnetic Compatibility (EMC), 2014 IEEE International Symposium on*, vol., no., pp.809-814, 4-8 Aug. 2014
22. Huray, P.G.; Pytel, S.G.; Millitz, R.I.; Hall, S.H., "Dispersion Effects from Induced Dipoles," in *Signal Propagation on Interconnects, 2006. IEEE Workshop on*, vol., no., pp.213-216, 9-12 May 2006

23. Shlepnev, Y., "Broadband material model identification with GMS-parameters," in *Electrical Performance of Electronic Packaging and Systems (EPEPS)*, 2015 IEEE 24th , vol., no., pp.155-158, 25-28 Oct. 2015
24. I.J. Bahl, R. Garg. *A designer's guide to stripline circuits*. Microwaves. January, 1978
25. Stephen H. Hall, Howard L. Heck. 'Advanced Signal Integrity for High-speed Digital Designs.' Jul 2008
26. David M. Pozar. *Microwave Engineering*. Addison Wesley. 1993
27. Shuai Jin; Ji Zhang; Jun Fan, "Optimization of the transition from connector to PCB board" *Electromagnetic Compatibility (EMC)*, 2013 IEEE International Symposium on
28. [https://en.wikipedia.org/wiki/Teardrop_\(electronics\)](https://en.wikipedia.org/wiki/Teardrop_(electronics))
29. Lei Hua; Bichen Chen; Shuai Jin; Marina Koledintseva; Jane Lim; Kelvin Qiu; Rick Brooks; Ji Zhang; Ketan Shringarpure; Jun Fan, "Characterization of PCB dielectric properties using two striplines on the same board", 2014 IEEE International Symposium on
30. Shuai Jin; Yaojiang Zhang; Yan Zhou; Yadong Bai; Xuequan Yu; Jun Fan, "Conducted-emission modeling for a high-speed ECL clock buffer", 2014 IEEE International Symposium on Electromagnetic Compatibility (EMC)
31. Yansheng Wang; Siqu Bai; Xinyun Guo; Shuai Jin; Yaojiang Zhang; Joakim Eriksson; Lijuan Qu; Jingyu Huang; Jun Fan, "Conducted-emission modeling for a switched-mode power supply (SMPS)", *Electromagnetic Compatibility and Signal Integrity*, 2015 IEEE Symposium on

VITA

Xinyao Guo received her B.S. degree of Electrical Engineering in May 2013 from Missouri University of Science and Technology. She joined EMC Lab in her B.S. last semester and continued her master's degree. She received her M.S. degree of Electrical Engineering in December 2016 from Missouri University of Science and Technology. She had co-op in Cisco CHG EMC/ SI design team from May to December 2015 and January to July 2016.

Her research interests included near field scanning technology, lossy material property, EMC and SI modeling, and high-frequency measurement.